Wnt/PCP controls spreading of Wnt/β-catenin signals by cytonemes in vertebrates

Benjamin Mattes[1,2], Yonglong Dang[2,3], Gediminas Greicius[4], Lilian T. Kaufmann[5], Benedikt Prunsche[6], Jakob Rosenbauer[7], Johannes Stegmaier[8,9], Ralf Mikut[8], Suat Özbek[10], G. Ulrich Nienhaus[2,6,11,12], Alexander Schug[8], David M. Virshup[4], Steffen Scholpp[1,2*]

[1] Living Systems Institute, School of Biosciences, College of Life and Environmental Science, University of Exeter, Exeter, EX4 4QD, UK
[2] Institute of Toxicology and Genetics (ITG), Karlsruhe Institute of Technology (KIT), 76021 Karlsruhe Germany
[3] Present address: Dept. of Molecular Neurobiology, German Cancer Research Center (DKFZ), 69120 Heidelberg, Germany
[4] Program in Cancer and Stem Cell Biology, Duke-NUS Medical School, Singapore 169857, Singapore.
[5] Institute of Human Genetics, University Hospital Heidelberg, Heidelberg, Germany
[6] Institute of Applied Physics, Karlsruhe Institute of Technology (KIT), 76049 Karlsruhe, Germany
[7] John von Neumann Institute for Computing, Jülich Supercomputing Centre, Forschungszentrum Jülich, Jülich, Germany
[8] Institute for Automation and Applied Informatics (IAI), Karlsruhe Institute of Technology (KIT), 76021 Karlsruhe, Germany
[9] Institute of Imaging and Computer Vision, RWTH Aachen University, Aachen, Germany
[10] Centre of Organismal Studies (COS), University of Heidelberg, Germany
[11] Institute of Nanotechnology (INT), Karlsruhe Institute of Technology (KIT), 76021 Karlsruhe Germany
[12] Department of Physics, University of Illinois at Urbana-Champaign, Urbana, IL 61801, USA.

Corresponding author: s.scholpp@exeter.ac.uk

Abstract

Signaling filopodia, termed cytonemes, are dynamic actin-based membrane structures that regulate the exchange of signaling molecules and their receptors within tissues. However, how cytoneme formation is regulated remains unclear. Here, we show that Wnt/PCP autocrine signaling controls the emergence of cytonemes, and that cytonemes subsequently control paracrine Wnt/β-catenin signal activation. Upon binding of the Wnt family member Wnt8a, the receptor tyrosine kinase Ror2 gets activated. Ror2/PCP signaling leads to induction of cytonemes, which mediate transport of Wnt8a to neighboring cells. In the Wnt receiving cells, Wnt8a on cytonemes triggers Wnt/β-catenin-dependent gene transcription and proliferation. We show that cytoneme-based Wnt transport operates in diverse processes, including zebrafish development, the murine intestinal crypt, and human cancer organoids, demonstrating that Wnt transport by cytonemes and its control via the Ror2 pathway is highly conserved in vertebrates.

Introduction

Wnt signaling regulates development and tissue homeostasis in multicellular organisms (Nusse and Clevers, 2017), including processes such as cell fate specification, proliferation, morphogenesis, and maintaining tissue integrity. Dysregulation of Wnt/β-catenin signaling has been causally linked to multiple diseases, with Wnt signaling being one of the most frequently dysregulated pathways in several cancer types (Anastas and Moon, 2013), including colorectal cancers, pancreatic cancer, and gastric cancers (Chiurillo, 2015; Madan and Virshup, 2015).

The Wnt signaling network consists of several branches that can be classified according to the receptors involved, and the specific signaling cascades they activate. Two major branches of this network are the β-catenin dependent pathway and the β-catenin independent Wnt/planar cell polarity (PCP) pathway (Niehrs, 2012). The β-catenin dependent pathway is triggered by the interaction of Wnt with Frizzled (Fzd) receptors and the co-receptor Lrp6 (Logan and Nusse, 2004). Wnt/β-catenin signaling regulates expression of target genes such as *axin2* and *lef1,* and tissue specific genes, and subsequently controls cell proliferation, as well as tissue patterning. In the β-catenin-independent Wnt/PCP pathway (Yang and Mlodzik, 2015), Wnt proteins bind to Frizzled and co-receptors such as the receptor-tyrosine kinase-like orphan receptor 2 (Ror2) to regulate cytoskeleton organization by actin polymerization and cell polarity (Grumolato et al., 2010; Ho et al., 2012; Oishi et al., 2003). To this end, small GTPases Rho, Rac1, and Cdc42 are regulated to control formation of filopodia and lamellipodia, cell motility and morphogenetic movements in vertebrates. Although the PCP pathway and β-catenin signaling generally act in a mutually repressive fashion, by competing for similar hub proteins, such as the effector protein Dishevelled (Dvl) (van Amerongen and Nusse, 2009), recent evidence suggests that PCP signaling can act – dependent on the context – either in opposition to, in concert with, or independently of β-catenin signaling.

The production and secretion of Wnt ligands requires lipid modification by the acyltransferase Porcupine (Porcn) followed by binding to Evi/Wls, which serves as a Wnt chaperone and facilitates its transport from the endoplasmic reticulum to the plasma membrane (Bartscherer and Boutros, 2008; Bänziger et al., 2006; Yu et al., 2014). From there, lipophilic Wnt is transported through the neighboring tissue to exert its long-range signaling activity. Extracellular binding proteins have been suggested to increase the solubility of Wg/Wnt in the aqueous extracellular space

and facilitate this activity (Mii et al., 2009; Mulligan et al., 2012). However, other studies point to membrane-associated mechanisms of Wg/Wnt delivery, without compromising its signaling capability (McGough and Vincent, 2016; Port and Basler, 2010; Stanganello and Scholpp, 2016). These trafficking routes include Wg/Wnt protein distribution on the plasma membrane of dividing source cells (Alexandre et al., 2014; Farin et al., 2016) and on actively migrating cells (Serralbo and Marcelle, 2014), or the dissemination of Wg/Wnt proteins on exovesicles (Panáková et al., 2005), or more specifically exosomes (Beckett et al., 2013; Gross et al., 2012; Korkut et al., 2009). Wg/Wnt proteins and their receptors are also transported on cell protrusions in various tissues. Lipid-modified Wnt proteins were found at the cell membrane on signaling filopodia – so-called cytonemes – in *Xenopus* and zebrafish (Holzer et al., 2012; Luz et al., 2014; Stanganello et al., 2015), whereas Fzd receptor proteins can be localized to filopodia in *Drosophila* and chicken (Huang and Kornberg, 2016; Sagar et al., 2015). In zebrafish, an analysis of cytonemes demonstrates that these are specialized filopodia, with stabilizing actin bundles at their cores, which serve as a main transport device for the β-catenin ligand Wnt8a during neural plate patterning (Stanganello et al., 2015). Wnt8a is loaded on cytoneme tips and transferred to the neighboring cells by direct cell-cell contact. At the contact sites, Wnt8a cytonemes induce Lrp6/Fzd receptor clustering into the Lrp6 signalosome to activate β-catenin signaling. Although the lengths and number of cytonemes is crucial for the β-catenin signaling range during embryogenesis (Stanganello et al., 2015), it is yet unclear what mechanism controls the formation of Wnt cytonemes in a tissue.

Here we show that Wnt8a can activate both the PCP pathway by interaction with Ror2 and the β-catenin pathway by interaction with Lrp6. This dual function allows Wnt8a to control its own route of dissemination: In the source cells, Wnt8a binds and activates the Ror2 co-receptor followed by activation of the PCP pathway. Wnt8a-PCP influences convergent extension (CE) movement and activates the small GTPase Cdc42, which leads to the outgrowth of signaling filopodia. Wnt8a is loaded onto these cytonemes, and is transported through the tissue to bind to the β-catenin specific co-receptor Lrp6 in the responding cells to activate the β-catenin pathway in a paracrine fashion in both PAC2 fish fibroblasts and HEK293T human embryonic kidney cells. Activation of the β-catenin pathway by Wnt cytonemes leads to target gene induction and regulates zebrafish neural plate patterning. Ror2-mediated Wnt

cytonemes also regulate the proliferation of human gastric cancer cells. Furthermore, we show that Wnt cytonemes induced by Ror2/PCP signaling are required for the maintenance of murine intestinal crypt organoids. We conclude that Ror2-regulated cytonemes are a critical transport route for Wnt proteins in vertebrates. The molecular mechanism for Wnt cytoneme formation illustrates the co-dependent interactions of the different branches of the Wnt signaling pathways.

Results

Tyrosine kinase Ror2 regulates filopodia emergence *in vitro*

Cumulative evidence indicates that Wnt signal molecules are lipidated and remain associated with membranes during secretion, action and degradation (Nusse and Clevers, 2017). Our previous work demonstrated that Wnt molecules can be distributed over 100 µm through a tissue via cytonemes (Stanganello et al., 2015). Manipulation of the length or number of Wnt cytonemes led to alterations in Wnt mediated tissue patterning and malformations of the zebrafish embryo. Therefore, we hypothesized that formation, emergence, and maintenance of cytonemes are tightly controlled. To identify potential cytoneme regulators, we performed a cell-culture-based genetic screen (Fig. 1A, Suppl. Fig. 4A-J) by co-expressing Wnt8a-GFP and GPI-anchored, membrane-bound mCherry (memCherry) in PAC2 cells together with arrayed cDNA clones from a Medaka cDNA library consisting of 229 kinases (Chen et al., 2014; Souren et al., 2009). 24 h post transfection, we quantified the length and number of signaling filopodia of ten fibroblasts per cDNA using automated filopodia detection software (Fig. 1B). The tyrosine-protein kinase transmembrane receptor Ror2 was found to stimulate both filopodia number per cell as well as average filopodia length above the 85th percentile (Fig. 1C,D).

To validate the screening results we co-transfected PAC2 fibroblasts with a zebrafish full-length Ror2 expression construct and GPI-memCherry as a membrane marker. The number and length of filopodia were measured in living cells (Fig. 1E). Ror2 expression significantly increased the average number and length of filopodia per cell (Fig.1F, Suppl. Fig. 1A,B). Ror2 requires homodimerization for transautophosphorylation and subsequent downstream signaling (Liu et al., 2007), which can be inhibited by over-expressing a kinase-dead construct. Transfection of the dominant-negative mutant Ror2^{3I} (Hikasa et al., 2002), caused a reduction in the number of protrusions as well as their average length, consistent with an essential

role of the Ror2 kinase activity in filopodia induction in PAC2 fibroblasts. The Rho GTPase Cdc42 is crucial for organizing the actin cytoskeleton to stabilize Wnt cytonemes (Stanganello et al., 2015) and is thought to be a downstream target of the Wnt/Ror2 pathway regulating filopodia (Schambony and Wedlich, 2007). To determine if Ror2-induced filopodia require Cdc42 function for assembling an actin scaffold we co-transfected Ror2 stimulated fibroblasts with dominant-negative $Cdc42^{T17N}$ (Nalbant et al., 2004). Blockage of Cdc42 function reduced filopodia formation significantly (Fig. 1E,F).

BAR-domain containing proteins mold membranes into tube-like filopodia. Insulin receptor tyrosine kinase substrate p53, IRSp53, is a BAR protein, as well as a Cdc42 effector, which connects filopodia initiation and maintenance by assembling the actin scaffold (Yeh et al., 1996). $IRSp53^{4K}$ contains four lysine residues mutated to glutamic acid in the actin-binding sites, inhibiting Cdc42-mediated filopodia formation (Disanza et al., 2013; Kast et al., 2014). $IRSp53^{4k}$ expression, like $Cdc42^{T17N}$ transfection, blocks Ror2-induced filopodia formation (Fig. 1E,F). Treatment of Ror2 expressing cells with ML141, a GTPase inhibitor for Cdc42/Rac1 (Surviladze et al., 2010), also caused a substantial reduction in both number and length of filopodia. Thus, Ror2 is a crucial regulator of filopodia in PAC2 fibroblasts, and filopodia depend on a Cdc42-mediated actin scaffold for their outgrowth and maintenance.

Cluster formation of Wnt8a and Ror2 is dependent on the CRD domain

Ror2 is a tyrosine kinase receptor that binds Wnt5a via its extracellular cysteine-rich domain (CRD) (Hikasa et al., 2002) and serves as a β-catenin independent Wnt co-receptor activating the PCP signaling pathway (Schambony and Wedlich, 2007). To investigate the interaction between Ror2 and the β-catenin ligand Wnt8a, we expressed fluorescently tagged Wnt8a and Ror2 proteins in the zebrafish embryo during gastrulation. The mRNA concentration of the injected fluorescent constructs was chosen in such a way that it did not induce phenotypic alteration at 24h (Suppl. Fig. 3A). Zebrafish *ror2* is expressed ubiquitously in early development, with its expression peaking during gastrulation between 2 and 9 hpf (Bai et al., 2014). Expression of the β-catenin Wnt ligand *wnt8a* is confined to the embryonic margin during zebrafish gastrulation, orchestrating patterning of the prospective neural plate (Kelly et al., 1995; Rhinn et al., 2005). Confocal microscopy on live specimens revealed that Wnt8a-GFP displays a punctate pattern in the cytoplasm and at the membrane, including cytoneme tips, whereas Ror2-mCherry without Wnt present is

uniformly distributed in the cell membrane (Fig. 2A, Suppl. Fig. 2A). When Wnt8a-GFP and Ror2-mCherry are co-expressed in the same cell, Ror2-mCherry accumulates in punctae along the membrane (Fig. 2A, Suppl. Movie 1). Correlated fluorescence intensity analysis of Wnt8a-GFP and Ror2-mCherry suggest both proteins predominantly co-localize in membrane associated clusters (Fig. 2B). This is supported by a Pearson-based correlation analysis of Wnt8a-GFP and Ror2-mCherry in embryonic tissue of a volume of 40 x 40 x 60 μm^3 (N=8, Suppl Fig. 2G). We found a similar intensity correlation between Wnt5b and Ror2 (Suppl. Fig. 2B,C). The CRD of Ror2 is crucial for interaction with Wnt ligands (Hikasa et al., 2002; Mikels et al., 2009). To exclude non-specific clustering of fluorescent fusion proteins, we used a Ror2 construct with a deletion in the Fzd-like CRD. We observed that Ror2-ΔCRD-GFP still localizes to the cell membrane and with Wnt8a-mCherry forming clusters therein. However, image profile analysis showed a marked reduction of the intensity peaks at the cluster site, indicating that Ror2-CRD is required for the interaction with Wnt8a (Fig. 2B).

Wnt8a and Ror2 co-migration and protein binding in signaling clusters

We further characterized Wnt8a/Ror2 protein-protein interactions *in vivo* using line-scanning fluorescence correlation spectroscopy (lsFCS; Suppl. Fig. 2D), which measures concentrations and diffusion coefficients of ligands and receptors in the presence of a membrane (Dörlich et al., 2015). We performed lsFCS analysis in two different spots, at a Ror2 positive membrane domain (spot 1) or at a Wnt8a/Ror2 membrane cluster (spot 2; Fig. 2C). A focused laser spot was scanned across the membrane for 390 s while the intensity was measured as a function of time. After compensation for membrane fluctuations, the intensity time traces were time-correlated. In spot 1, we found intensity fluctuation from Ror2-mCherry emission (Fig. 2D). A fit of the autocorrelation function revealed a receptor concentration (area density) C_r = (37 ± 3) μm^{-2}. The diffusion coefficient, D = (0.28 ± 0.03) $\mu m^2\ s^{-1}$, is similar to values found for LRP6 receptors in the plasma membrane (Dörlich et al., 2015). There was no clear emission from Wnt8a-GFP molecules in spot 1. By contrast, lsFCS on spot 2 revealed clear autocorrelations in both color channels (Fig. 2E), indicating the presence of both Wnt8a-GFP and Ror2-mCherry at this site. We found a dual-color cross-correlation between Wnt8a-GFP and Ror2-mCherry (Fig. 2E), indicating concerted intensity fluctuations in both color channels, which arise from their co-diffusion in the plasma membrane due to binding. Therefore, the cross-

correlation lsFCS data provide clear evidence of complex formation between Wnt8a and Ror2. Furthermore, the low diffusion coefficient of the bound species, D = (0.02 ± 0.01) $\mu m^2 s^{-1}$, indicates that the complexes diffuse as large clusters.

We have previously shown that Fzd7 also interacts with Ror2 and enhances Ror2-mediated signaling during *Xenopus* gastrulation (Brinkmann et al., 2016), suggesting Fzd7a could be a part of the Wnt8a/Ror2 cluster in zebrafish. To test this, we overexpressed Ror2-mCherry, Fzd7a-CFP and Wnt8a-GFP and found co-localization of all three proteins in the cell membrane (Suppl. Fig. 2E,F).

From our data, we conclude that Wnt8a interacts with Ror2 by binding to its CRD. Wnt8a and Ror2 co-migrate and form dense protein clusters. The data suggest that the Wnt8a/Ror2 clusters are in close steric contact with other components of the Wnt signaling complex including Fzd7a.

Wnt8a/Ror2 signaling activates the PCP pathway

The interaction of Wnt8a with Ror2 could trigger non-canonical PCP signaling via the Ror2 pathway. PCP signaling plays a role in regulating tissue migration during gastrulation (Tada and Heisenberg, 2012). PCP signaling via Ror2 activation regulates collective cell migration towards the embryonic midline, which is most pronounced in the mesodermal germ layer in zebrafish (Bai et al., 2014). We utilized this classical PCP controlled process to observe the involvement of Wnt8/Ror2 in non-canonical signaling. CE can be visualized by condensation of the *no tail* (*ntl*) positive notochordal plate at the embryonic midline at 11 hpf (Fig. 3A). To this end, we over-expressed the Ror2 receptor, which alone had a very small effect on the establishment of the *ntl* expression domain (for classification see Suppl. Fig. 3B). However, over-expression of Wnt8a leads to a broadening and shortening of the *ntl* expression domain. This phenotype is reminiscent of Wnt5b activation. A similar phenotype was observed when Wnt8a and Ror2 were co-expressed. Categorization of the phenotypes suggests that the co-activation of Ror2/Wnt8a or Ror2/Wnt5b have similar effects (Fig. 3B). Inhibition of Ror2 function by either $Ror2^{3I}$ expression or a Morpholino-based Ror2 knock-down also led to CE defects. Our data suggest that Fzd7a may be a member of the Ror2-Wnt8a signaling complex (Suppl. Fig. 2E,F). We found an enhanced broadening of the embryonic midline if Wnt8/Fzd7a and Wnt8a/Fzd7a/Ror2 were overexpressed (Suppl. Fig. 3C). This suggests that endogenous Ror2 is expressed at high levels already, and the available Wnt ligand

concentration is the key quantity controlling step for PCP signaling during zebrafish CE.

During CE, cells intercalate in the notochordal plate (convergence), push previously adjacent cells apart, and lengthen the field along the AP axis (extension) (Glickman et al., 2003). We investigated the shape of the notochord cells in embryos with ectopically expressing Wnt8/Ror2 signaling. We found that the cells had a less bipolar shape and displayed a more circular form in embryos with Wnt8/Ror2 signaling, reminiscent of Ror2 activation by Wnt5a (Figure 3C,D), suggesting that mediolateral narrowing of axial mesoderm is reduced.

Activation and inhibition of the PCP signaling pathway leads to a similar phenotype (Tada and Heisenberg, 2012). Therefore, we were unable to distinguish how Wnt8a/Ror2 alters PCP signaling. During *Xenopus* gastrulation, Wnt5A activates Ror2 downstream signaling, leading to Cdc42 activation, JNK phosphorylation, and, ultimately, the enhancement of ATF2 transcription (Hikasa et al., 2002; Schambony and Wedlich, 2007). To test if zebrafish Wnt8a is able to activate Ror2 signaling, we used a reporter assay with an ATF2 responsive element driving luciferase expression in *Xenopus* embryos (Brinkmann et al., 2016; Ohkawara and Niehrs, 2011). Wnt8a co-expressed with Ror2 produced a greater than five-fold induction of the ATF2 reporter in *Xenopus* (Fig. 3E). Co-expression of Wnt5A/Ror2 leads to a similar activation of reporter expression, whereas expressed Ror2 without a co-expressed ligand did not alter expression of the ATF2 reporter. We determined if the kinase domain of Ror2 is required for Wnt8a dependent activation of the PCP pathway by overexpressing Wnt8a together with dominant-negative Ror2^{3I} and observed a reduction of ATF2 reporter activation compared to activation of Wnt8a/Ror2.

Taken together, our data indicate that Wnt8a serves as a ligand for the receptor Ror2 and induces PCP signaling upon binding. Thus, ectopic over-expression of Wnt8a modulates cell movements and cell morphology in zebrafish and gene transcription in *Xenopus*.

Ror2 induces Wnt-cytonemes during zebrafish neural patterning.

To study the dynamics of filopodia formation in the Wnt8a positive germ ring during normal development in zebrafish (Suppl. Movie 2), we quantified signaling filopodia during gastrulation in live embryos. In confocal image stacks, filopodia were traced using a semi-automatic live wire approach (Barrett and Mortensen, 1997). A

precise measurement of filopodia protrusion lengths in 3D was obtained using manually selected nucleation start points and filopodia end points. We found that the number of filopodia significantly increase from 4 – 6hpf, which comprises the neural plate patterning phase (Fig. 4A,B). This coincides with increasing Ror2 expression levels during zebrafish development (Bai et al., 2014). We determined if formation of these filopodia was dependent on Ror2 function by manipulating Ror2 signaling and measured germ ring cell filopodia number at 6 hpf. We found only a modest increase of filopodia number if Ror2 was activated, suggesting Ror2 itself is not rate-limiting (Fig. 4C,D). However, when Ror2 function was reduced by over-expression of $Ror2^{3I}$, we observed a significant reduction in filopodia number. We conclude that Ror2 signaling is required for filopodia induction of embryonic marginal cells during zebrafish development.

We speculated that Ror2 might influence formation of filopodia carrying Wnt8a protein - Wnt8a-cytonemes - during zebrafish gastrulation. To visualize these cytonemes we generated cell clones at the embryonic margin expressing Wnt8a-GFP and memCherry. Wnt8a-GFP clusters were seen in the cell membrane and cytoneme tips of germ ring cells (Fig. 4E). Statistically more filopodia carrying Wnt8a-GFP clusters on their tips were detected upon Ror2 overexpression within cells (Fig. 4E,F). Conversely, we found a significant reduction in the number of cytonemes in Ror2 deficient marginal cells. Wnt8a-GFP is still present at the plasma membranes of cells with compromised Ror2 function, suggesting that intracellular routing of Wnt8a from the producing organelles to the cell membrane is independent of Ror2-dependent cytonemal transport. Filopodia without detectable Wnt8a seemed to be unaffected by Ror2 signaling in zebrafish (Fig. 4F). This suggests a function of Ror2 in regulating a specific subset of filopodia, those carrying Wnt8a - the Wnt cytonemes - in the zebrafish embryo *in vivo*.

Based on these findings, we hypothesized that Ror2 function in the Wnt source cells is crucial for Wnt dissemination via cytonemes. To test the consequences of altered Ror2 signaling quantitatively, we used a simulation of morphogen distribution via cytonemes (Stanganello et al., 2015). The simulation takes into account ligand transport by cytonemes, ligand decay and migration of epiblast cells using a Monte Carlo based direct event simulation approach. Employing cytonemes as the exclusive transport mechanism from the producing cell group to the target cell group, and assuming an unlimited source of the ligand, we found that cytonemes can

distribute Wnt8a in a graded manner in the dynamically evolving target tissue (Fig. 4G). We tested two scenarios with varying cytoneme number, based on our *in vivo* measurements after alteration of Ror2 function (Fig. 4F). We found that ligand concentration within the morphogenetic field depends on the appearance of the cytonemes (Stanganello et al., 2015). We found that increasing the number of cytonemes per cell (by the experimentally determined factor of 1.61) after expression of Ror2 and Wnt8a in the source cells, leads to an enhanced ejection (187%) of the ligand into the target tissue compared to the Wnt8a producing cells (Fig. 4G). Consistently, by using the measured cytoneme parameters after blockage of Ror2 function (number scaled by 0.388), we found a decrease to 36% of the Wnt8a concentration compared to the WT situation and a smaller range of the morphogen gradient within the tissue. These data suggest that Ror2 signaling can specifically regulates the number of Wnt positive cytonemes *in vivo* and thus represents a cytoneme specific regulator. Furthermore, based on the simulations, we predicted a strong decrease in the range of Wnt signal activation in the neighboring tissue if Ror2 function is compromised in the Wnt8a source cells.

Ror2 presents Wnt8a to the target cell to induce ligand-receptor cluster.

Next we asked how Wnt8a and Ror2 interact to facilitated cytoneme-mediated transport. Therefore, we performed a high-resolution imaging approach in the developing zebrafish embryo by over-expressing tagged constructs (Fig. 5). The high-sensitivity of the image-based approach allowed us to reduce the expression levels of the tagged construct significantly and morphological alterations of the embryonic phenotype was not observed at 24hpf (Suppl. Fig. 3A). By a time-lapse analysis, we observe the formation of Wnt8a-GFP positive clusters, which transit in the plasma membrane of the secreting cell (Fig. 5B). Then, Wnt8a co-localizes with Ror2 at the plasma membrane suggesting Wnt8a-Ror2 cluster induction (Fig. 5C) as previously described (Fig. 2A,B). These clusters initiate cytoneme formation and, consequently, they decorate the tip of the outgrowing cytoneme. The cytoneme contact the target cell and Wnt8a-Ror2 forms a cluster at the receiving cell (Fig. 5C, Suppl. Movie 3). Within minutes, this clusters is endocytosed into the target cell. We were wondering if Wnt8a-Ror2 induces the Wnt signaling cascade in the target cell. Therefore, we analyzed Lrp6-signalosome formation at the plasma membrane of the target cell by induction of a Wnt8a secreting cell clone and aLrp6-expressing receiving cell clone (Fig. 5D). We find that cytonemal Wnt8a-mCherry induces Lrp6-

GFP cluster formation at the membrane of the target (Fig. 5E,F). We hypothesized that the source cell presents Wnt8a by clustering the ligand on Ror2 positive cytonemes. Indeed, we observe a Lrp6-GFP cluster that at the contact points of Ror2-positive cytonemes (Fig. 5E). The following dynamics of Lrp6-signalosome has been described recently in zebrafish development (Hagemann et al., 2014).

Therefore, we conclude that Ror2 clusters on cytoneme tips to act as a platform to present Wnt8a to the target cell and induce the Wnt signaling cascade therein.

Ror2 regulates PCP signaling in the Wnt source cells and β-catenin signaling in the Wnt receiving cells

Based on our simulations, we speculated that Ror2 signaling may have a function in Wnt ligand trafficking and, consequently, in paracrine β-catenin signaling during zebrafish gastrulation. To test this, we over-expressed Ror2 and analyzed its effect on CE processes (via PCP signaling) and, simultaneously, on neural plate patterning (via β-catenin signaling; Suppl. Fig. 6A) during embryogenesis. Over-expression of Ror2 by injection of low levels of mRNA did not induce gross morphological changes in zebrafish embryos, consistent with our findings that Ror2 without a suitable ligand only mildly impacts on PCP mediated processes (Fig. 3A,C,E). Over-expression of Wnt8a resulted in a substantial alteration in neural plate patterning as described above, with β-catenin signaling being activated in the entire neural plate, marked by ubiquitous *axin2* expression at 6 hpf (Fig. 6A). As a consequence, we observed posteriorization of the developing nervous system, observed as an anterior shift of the *fgf8a* positive midbrain-hindbrain boundary (MHB) at 9 hpf and a loss of the anterior *pax6a* positive forebrain at 26 hpf. In embryos co-expressing Wnt8a together with Ror2, we still observed the posteriorization phenotype in the neural plate and, in addition, we found that CE is compromised, as the neural plate does not converge to the midline and, consequently, the expression domains of *fgf8a* at the MHB showed a pronounced gap.

We compared these observation to embryos expressing the β-catenin independent ligand Wnt5a, and Wnt5a together with Ror2. Ror2 mediated Wnt5a signaling induces CE in *Xenopus* (Hikasa et al., 2002) and represses β-catenin signaling in mouse embryos (Mikels et al., 2009). In both settings, we observed a strong effect on CE movement in the zebrafish embryo. In addition, Wnt5a/Ror2 over-expression led to reduced β-catenin signaling, causing a reduction in target gene expression (*axin2*) and anteriorization of the neural plate, leading to a posterior

shift of *pax6a* expression in the forebrain. We conclude that Wnt8a can activate β-catenin signaling and PCP signaling via the Ror2 receptor during zebrafish development. We showed that Wnt5b/Ror2-mediated PCP signaling represses Wnt/β-catenin signaling. We hypothesized that Wnt8a function depends on the route of secretion. However, global over-expression did not differentiate between autocrine and paracrine Wnt8a signaling mechanisms and on subsequent downstream activation.

To separate Wnt-producing from Wnt-receiving cells, we performed a co-cultivation assay using HEK293T cells, which are typically Wnt-Off due to low endogenous expression of Wnt ligands (Voloshanenko et al., 2017). Cytoneme regulators were transfected into HEK293T source cells (Wnt-producing cells) and co-cultivated with HEK293T cells expressing the SuperTOPFlash TCF/Wnt reporter, with seven TCF responsive elements hooked up to nuclear mCherry (7xTRE-NLS-mCherry (Moro et al., 2012), Suppl. Fig. 6B). Ror2 transfection into source cells did not alter the induction of 7xTRE-nucRFP in the receiving cells (Fig. 6B,C). However, Wnt8a-producing cells lead to activation of signaling activity in the HEK293T reporter cells. Reporter expression was further enhanced (147.3% compared to Wnt8a transfected source cells) when Wnt-producing cells co-expressed Wnt8a and Ror2, indicating a synergistic interaction between Wnt8a and Ror2 (Fig. 6D). Co-transfection of Wnt8a with dominant-negative Ror2^{3l} resulted in a 34.6% decrease in reporter activation, compared to Wnt8a transfected source cells. These findings support our simulations regarding the available Wnt8a concentration in the target tissue after alteration of Ror2-dependent cytoneme appearance (Fig. 4G). We conclude that Wnt8a can be transmitted via Ror2 dependent cytonemes in HEK293T cells, while Wnt5b and Wnt5b/Ror2 transfections were unable to activate the β-catenin signaling reporter in neighboring cells (Fig. 6D).

To test whether Ror2-mediated Wnt cytonemes affect β-catenin dependent target gene activation in neighboring cells *in vivo,* we generated small-source clones by microinjecting cytoneme regulator mRNAs at the 16-cell stage (Suppl. Fig. 6C). By mid-gastrulation, the source cells were distributed over an area of the embryo and intermingled with WT host cells, generating many responding cells around a few source cells. At 6 hpf, we analyzed the transcriptional profile of the embryos for the β-catenin target genes *axin2* and *lef1*. Embryos with cells over-expressing Ror2 or Ror2^{3l} showed no alteration in *axin2* or *lef1* expression (Fig. 6D). However, source

cells over-expressing Wnt8a resulted in a significant increase in β-catenin dependent target gene expression, which was not further enhanced by Ror2 addition. However, blockage of cytoneme formation in the Wnt8a source cells by co-expression of Ror2^{3I} led to a significant reduction of β-catenin target gene induction in neighboring cells. Blockage of filopodia *per se* by over-expression of the dominant-negative form of IRSp53^{4K} caused a similar reduction of activation of *axin2* and *lef1* expression in embryos. This suggests that, during zebrafish gastrulation, the majority of Wnt8a protein is transmitted via cytonemes and that the formation of these Wnt cytonemes is Ror2 dependent.

Ror2-dependent cytonemes in cancer cell lines and intestinal organoids

Over-activation of canonical β-catenin signaling can be identified in one-third of gastric cancers (Chiurillo, 2015). β-catenin signaling is essential for self-renewal of gastric cancer stem cells, leading to Wnt-mediated resistance to apoptosis, which may be responsible for recurrences in these tumors. The β-catenin-independent branch plays a similarly important role in cancer progression: The key ligands Wnt5a and Ror2 are upregulated in various gastric cancers, regardless of the histological phenotype. To determine if Wnt ligands are transported on cytonemes between gastric cancer cells, we used the gastric cancer (GC) cells lines MKN7, MKN28 and AGS. Transfected Wnt8a-mCherry localized on filopodia in GC cell lines (Fig. 7A, Suppl. Fig. 7). Forced expression of Ror2 led to a strong increase of the number of filopodia in GC cells (Fig. 7B,C), whereas, there was a significant reduction of the cumulative filopodia length in cells expressing dominant-negative Ror2^{3I} (Fig. 7C), indicating that Ror2 also control filopodia formation in GC cells.

We focused on AGS cells as they show highly dynamic formation and retraction of filopodia, are particularly receptive to Ror2 manipulation, express Wnt1 at constant high levels, and, thus, have high endogenous β-catenin activity, which has been linked to the increased proliferation rate of this cell line (Mao et al., 2014). To assess whether cytoneme-mediated Wnt transport influences AGS cell behavior, and specifically proliferation, we co-cultivated Ror2 transfected cells with cells carrying the nuclear marker nucRFP. Cells over-expressing Ror2 significantly increase cell proliferation in neighboring AGS cells (Fig. 7D,E). Co-expression of the specific filopodia inhibitor IRSp53^{4K} dampened the increased proliferation rate induced by Ror2 expression. Inhibition of Wnt signaling by the tankyrase inhibitor IWR1 abrogated the stimulatory effect of Ror2 expression, confirming that the Ror2 effect is

due to increased Wnt signaling. We conclude that Wnt is moved on cytonemes between GC cells to stimulate Wnt/β-catenin signaling and proliferation in neighboring cells. Abrogation of this transport route has a similar consequence as inhibition of Wnt signaling *per se* – it leads to reduced proliferation.

As the intestinal crypt requires a constant supply of Wnt signaling for tissue homeostasis (Beumer and Clevers, 2016; Kuhnert et al., 2004; Pinto et al., 2003; Sailaja et al., 2016) we asked if Wnt cytonemes operate in the mouse intestinal crypt. *In vivo*, subepithelial myofibroblasts provide the major source of physiologically relevant Wnts, which maintain the crypt *in vivo* (Kabiri et al., 2014; Valenta et al., 2016). It has been further demonstrated that these PdgfRα positive myofibroblasts regulate the intestinal stem-cell niche by Wnts and RSPO3 (Greicius et al., 2018). The intestinal myofibroblasts form a large amount of filopodia (Fig. 7F). The formation of filopodia is inhibited by siRNA-mediated knock-down of Ror2. We used an organoid formation assay to analyze the requirement of Wnt signaling filopodia in the intestinal crypt. We used Wnt deficient Porcn$^{-/-}$ crypt cells, co-cultivating them with Wnt3a-secreting L cells to grow Wnt-deficient crypt organoids. Co-culture of WT myofibroblasts with Wnt-deficient crypt cells leads to induction and maintenance of crypt organoids (Kabiri et al., 2014). These myofibroblasts extend filopodia to engulf crypt organoids (Suppl. Fig. 7C). If Ror2 is knocked down in the Wnt-producing myofibroblasts we observed a substantial decrease in the number of organoids (Fig. 7G). This suggests that Wnt signaling transport on Ror2-dependent cytonemes from the myofibroblasts is crucial for induction and maintenance of the intestinal crypt. We conclude that cytonemes are vital for Wnt protein dissemination in vertebrates and their appearance is regulated by Ror2-mediated PCP signaling.

Discussion

Cytonemes transport signaling molecules

Cytonemes are actin-based filopodia that transport an array of signaling molecules and their receptors, facilitating juxtacrine signaling. Their appearance is highly dynamic during development (Gradilla and Guerrero, 2013; Kornberg and Roy, 2014; Stanganello and Scholpp, 2016). A continuous adjustment of the number, length, rate of formation, direction, and retraction of cytonemes is crucial to regulate exchange of signaling proteins within a tissue. However, how cytoneme formation is controlled remains unclear. Cytonemes change in response to signaling protein

levels in the source cell (Sato and Kornberg, 2002; Stanganello et al., 2015) suggesting that cytoneme formation is linked to signal production. A signaling pathway influencing cytoneme emergence is the Wnt signaling network. We have found that cytoneme initiation is linked to Wnt8a production. Wnt8a activates the PCP signaling pathway in ligand-producing cells and, in turn, PCP induces cytonemes, which can be loaded with Wnt protein. Data from *Drosophila* show that cytonemes require the PCP components Prickle and Vangl, which are essential for Fgf and Dpp positive cytonemes in the air sac primordium (Huang and Kornberg, 2016). However, Prickle/Vangl modulate heparin proteoglycan content in the extracellular matrix to allow cytoneme outgrowth. In contrast, we found that Wnt8a activates the PCP pathway via interaction with the Ror2 receptor to initiate cytoneme formation. Our *in vivo* analysis suggests that activation of Ror2 in the zebrafish embryonic margin is necessary and sufficient for formation of Wnt cytonemes, as other filopodia remain unperturbed. We conclude that Ror2 is a specific cytoneme regulator.

Ror2 in filopodia formation

Ror2 is a member of the family of orphan receptor tyrosine kinases, possessing an extracellular Fzd-like CRD, a cytoplasmic tyrosine kinase domain, and a proline-rich domain (PRD) (Yoda et al., 2003). Ror2 plays crucial roles in developmental morphogenesis in vertebrates. Ror2-deficient mice exhibit skeletal, genital, and cardiovascular abnormalities caused by disrupted CE movements during gastrulation (Oishi et al., 2003; Takeuchi et al., 2000). Ror2 is required for filopodia formation and XWnt5a-induced cell migration in *Xenopus* (Nishita et al., 2006). Irrespective of stimulation by Wnt proteins, ectopic expression of Ror2 can induce filopodia formation by actin polymerization via coupling of the Ror2-PRD to the actin-binding protein Filamin A. Our *in vitro* data show that Ror2 induces filopodia formation in PAC2 fibroblasts, myofibroblasts and gastric cancer cells. Moreover, we show that Ror2 is crucial for Wnt cytoneme formation *in vivo,* and it is known to contribute to cytoskeleton remodeling and JNK activation in migrating cells (Oishi et al., 2003). We have previously shown that Wnt cytonemes require Cdc42 function to stabilize the intracytonemal actin skeleton (Stanganello et al., 2015). Here we demonstrate that Ror2-dependent cytonemes also require Cdc42 function for formation and maintenance of the actin scaffold. Our data are supported by an analysis of CE movement in *Xenopus*: Co-expression of $Cdc42^{T17N}$ rescues XRor2-induced CE

alterations (Hikasa et al., 2002), suggesting that Ror2 regulates Cdc42-dependent processes.

Ror2 and Wnt ligands

Ror2 acts as a receptor for Wnt5A in mice (Mikels et al., 2006). In *Xenopus*, Wnt5A/Ror2 activates the PCP signaling pathway, including transcription of ATF2 and PAPC (Schambony and Wedlich, 2007). Although there is *in vitro* evidence that multiple Wnts can associate with the CRD domain of Ror2, only a few Wnts have been demonstrated to elicit Ror2 activation *in vivo*. For example, Wnt1 and Wnt3a bind to the CRD domain of Ror2 (Billiard et al., 2005) yet neither altered receptor activity as assessed by levels of Ror2 autophosphorylation. *Xenopus* Wnt8 binds to the ectodomain of Ror2 (Hikasa et al., 2002) but it is not known if XWnt8 induces Ror2 signaling. In zebrafish, evidence suggest Wnt11 is a potential binding and signaling partner for Ror2 (Bai et al., 2014). Wnt11 activates Ror2 to modulate CE during zebrafish gastrulation. We have observed that Wnt8a co-localizes with Ror2 in cytonemes. Although tagged constructs have been examined at very low concentration, this does not necessarily imply correct subcellular localization. However, our results are in line with studies on endogenous Wnt8a localization on cytonemes (Stanganello et al., 2015) and with studies on Ror2 localization on filopodia in mouse (Paganoni and Ferreira, 2003; Laird, et al., 2011) and in Xenopus (Nishita, et al. 2006; Brinkmann et al., 2014). We have further observed that Wnt8a binds and activates Ror2 signaling *in vitro* and *in vivo*. It is possible that other β-catenin independent Wnts, such as Wnt5a and Wnt11, might induce Ror2 cytonemes to regulate β-catenin Wnt ligand trafficking and thus β-catenin signaling. Wnt5A and Wnt11 are known to regulate dorso-ventral patterning of the neural tube and somites in mice (Andre et al., 2015). However, the observed patterning defect and AP axis shortening in Wnt5A/Wnt11 double knockout mice was explained by migration alteration of the axial mesoderm.

Interaction of the Wnt signaling branches

Binding of Wnt proteins to their cognate Frizzled receptors activates several distinct signaling pathways, including the canonical Lrp6/β-catenin-dependent and the non-canonical Ror2/β-catenin-independent PCP pathways (Niehrs, 2012). According to the conventional classification, Wnt1, Wnt3a, and Wnt8a belong to the β-catenin dependent Wnt signaling proteins, whereas Wnt5a and Wnt11 are representatives of the β-catenin independent Wnt signaling proteins (Kikuchi et al.,

2011). Activation of the Ror2/PCP signaling branch is assumed to repress the β-catenin signaling branch (Niehrs, 2012). Both Wnt signaling branches use the same hub proteins as intracellular effectors, which may lead to competition and mutual repression. For example, Wnt5a, which preferentially activates PCP signaling, competes with Wnt3a for Fzd2 and thus inhibits the β-catenin-dependent pathway (Sato et al., 2010). Furthermore, in *C. elegans*, Ror2 is thought to act by sequestering β-catenin Wnt ligands, a function independent of its intracellular domain (Green et al., 2007). In tissue culture, intracellular Ror2 signaling represses β-catenin signaling via its tyrosine kinase activity (Mikels et al., 2006) and interaction with Dvl (Witte et al., 2010). Furthermore, intracellular binding partners such as Tak1 interact with the C-terminal region of Ror2 to further inhibit Wnt/β-Catenin signaling (Winkel et al., 2008). However, recent work reported that Ror2 signaling is able to enhance β-catenin mediated signaling and proliferation in several tumor types (Rasmussen et al., 2013; Roarty et al., 2017; Yan and Lin, 2008). These apparently contradictory results could be explained by cross-regulation of Ror2 and the β-catenin signaling being influenced by tissue heterogeneity, e.g. during tumor progression (Roarty et al., 2017), where Ror2-expressing tumor cells regulate the spatial distribution, duration, and amplitude of Wnt/β-catenin signaling within a tumor, depending on the repertoire of Wnt signaling components present. Our data provide a mechanistic explanation of this effect. Although we cannot rule out the possibility of Ror2 activation within the Wnt source cells, we hypothesize that the Ror2/PCP signaling pathway is activated in an autocrine fashion based on our observations of the behavior of individual cells in cell culture and in the embryo. We further provide evidence that Ror2/PCP-dependent signaling is crucial for cytoneme emergence in Wnt source cells. Then, cytonemes transmit Wnt ligands to neighboring cells to activate juxtacrine β-catenin signaling. We demonstrate the importance of separating Wnt-producing from Wnt-receiving cells by showing that Ror2-mediated Wnt transport is required for controlling cell proliferation in AGS gastric cells. AGS cells express Wnt ligands such as Wnt1, display a high endogenous β-catenin level, and show enhanced proliferation (Mao et al., 2014). The anti-cancer drug salinomycin inhibits β-catenin signaling by inducing degradation of the Wnt co-receptor Lrp6, resulting in reduced proliferation. Autonomous activation of PCP signaling via Ror2 represses β-catenin signaling and reduces proliferation in AGS cells (Yan et al., 2016), suggesting that activation of PCP signaling could be used as a further strategy to inhibit uncontrolled

proliferation of gastric tumors. However, gastric tumors display a high degree of tissue heterogeneity and we find that Ror2 can also enhance β-catenin signaling and consequently cell proliferation. Our experimental approach is fundamentally different compared to the former analysis: Wnt producing cells and Wnt receiving cells are treated separately. We find that Ror2 activation in the Wnt producing cells increases proliferation in the Wnt receiving cells. This hypothesis is supported by recent findings showing that Wnt-Ror2 positive mesenchymal cells promote gastric cancer cell proliferation if co-cultivated (Takiguchi et al., 2016).

Cytonemes are a general carrier for Wnt protein dissemination

Here, we describe Ror2/PCP-induced cytonemes as transport carrier for Wnt8a in zebrafish. In cell culture experiments, we use PAC2 fibroblasts and HEK293T cells to provide further evidence for the importance of Ror2-dependent cytonemes in Wnt trafficking. In addition, we show that human gastric cancer cells AGS, which primarily express the Wnt ligand Wnt1, process paracrine Wnt signaling via cytonemes, which are influenced by Ror2 signaling. Finally, we use murine intestinal stroma cells, which express Wnt2b to maintain the Wnt gradient operating in the intestinal crypt (Aoki et al., 2016; Kabiri et al., 2014). We provide further evidence that Wnts from intestinal stroma utilize Ror2-dependent cytonemes for their transport. In summary, we show that autocrine PCP pathway activation via Ror2 induces Wnt cytonemes in the Wnt source cell to transmit Wnt to the neighboring cell to activate paracrine Wnt/β-catenin signaling. We propose cytonemes as an general mechanism for mobilization of Wnt ligands in tissue homeostasis as well as in development in vertebrates.

Acknowledgements

This project was funded by the Living Systems Institute, the University of Exeter and the Boehringer Ingelheim Foundation to SS. Studies in the DMV lab are supported by the National Research Foundation of Singapore and National Medical Research Council under its STAR Award Program. JR and AS were supported by the Impuls- und Vernetzungsfond of the Helmholtz Association. GUN was funded by the Deutsche Forschungsgemeinschaft (SFB 1324, projects A6 and Z2, GRK2039) and Helmholtz Association Program STN. For technical assistance, we would like to thank Donya Shapoori (RTqPCR analysis), Julia Schuller and Melanie Merkel (Fzd7/Ror2 interaction studies); Trevor Dale and Toby Phesse (ECSCRI, Cardiff

University) for providing the gastric cancer cell lines; Francesco Argenton (Uni Padova), Steve Wilson & Masa Tada (UCL) and Yashuiro Minami (Kobe University) for providing plasmids and Gáspár Jékely (LSI Exeter) for comments to the manuscript. We would like to thank the Aquatic Resources Centre (ARC) and the BioImaging Centre, Exeter for excellent technical support.

Author Contributions

BM and SS designed, performed and analyzed all experiments except where noted and wrote the manuscript. YD screened the kinase cDNA library, GG and DMV performed the intestinal organoid studies, LTK and SÖ performed the ATF2 reporter assay, BP and GUN contributed the FCS data, JR and AS designed and performed the simulations, JS and RM developed the cytoneme analysis software.

Declaration of Interests

The authors declare no competing interests.

Figure legends

Figure 1: Kinase Screen and automated image-analysis identifies the receptor tyrosine kinase Ror2 as a potential cytoneme regulator upstream of Cdc42. (A) Schematic workflow of the cDNA kinase screen. Wnt8a-GFP and a membrane bound mCherry was co-transfected with kinase library genes in a 96-well plate. Images were acquired automatically and analyzed for filopodia length and numbers by a filopodia detection software. (B) Automated Image analysis software detects and counts filopodia of single cells using the memCherry signal and quantifies their length by automatically tracing the tips back to the cell body. Scale bar represents 15µm. (C, D) Diagram illustrating transfected kinase genes on x-axis and their relative filopodia number/cell and length. Each bar represents one of 229 kinases, sorted ascending by its value. The blue line indicates the 85^{th} percentile (number: 1.20, length: 1.25). The position of Ror2 in the diagram is highlighted by the red line (number: 1,20, length: 1.47). (E) Quantification of filopodia in PAC2 cells 24h after transfection or inhibitor treatment. memCherry was transfected together with indicated constructs. Scale bar represents 10µm. (F) Boxplot for cumulative filopodia length of cells transfected with indicated constructs measured by ImageJ. Centre lines show the median; box limits indicate the 25th and 75th percentiles as determined by R software; whiskers extend 1.5 times the interquartile range from the 25th and 75th percentiles, outliers are represented by dots. Significance level as indicated: ***=P<0.001, **=P<0.01, =P<0.05. Data meet the assumption that the length of filopodia is significantly different in the analyzed groups by one-way ANOVA with a $P=5.79*10^{-99}$, confidence interval 95%, F value=118, and df=1047.

Figure 2: Image-based protein interaction analysis highlights Ror2s implication in Wnt8a binding and cluster formation. (A) At the 8–16-cell stage, single blastomeres of zebrafish embryos were microinjected with 25ng/µl mRNA of indicated constructs to generate cell clones at 50% epiboly for confocal microscopy analysis. Imaging visualizes co-localization of proteins at a single confocal plane including high-magnification of clusters. (B) Co-localization channel by fire LUT and the intensity plot profile were generated in ImageJ. Intensity plots show one individual measurement along the membrane (left plot, orange arrows) and the average of measurements across the membrane incl. SEM (right plot, light blue arrows). Graph represents 10 membrane clusters acquired from 5 different cells of 2 different embryos per treatment. (C) Close-up of a 6 – 8 hpf live zebrafish embryo showing

schematically how two-color two-foci line-scanning fluorescence correlation spectroscopy (2c2f lsFCS) data were taken by laser scanning perpendicular to the membrane (white lines) to collect data in the absence (spot 1) or presence (spot 2) of Wnt8a-GFP. Embryos were mounted in agarose and injected with Wnt8a-GFP and Ror2-mCherry. (D) Autocorrelation functions of Ror2-mCherry (red) and Wnt8a-GFP (green) (symbols) and model fit (line) measured in spot 1. The total time of the measurements was 390s. Importantly, there is no Wnt8a-GFP at this position as shown by the lacking autocorrelation in the green channel. Error bars represent standard deviations from two measurements. (E) Autocorrelation functions of Ror2-mCherry (red) and Wnt8a-GFP (green) and the dual-color cross-correlation (blue) (symbols) and model fits (lines) measured in spot 2. Here, Wnt8a-GFP is present, and a high cross-correlation amplitude indicates co-diffusion of bound Ror2-mCherry and Wnt8a-GFP. Error bars indicate standard deviations from two measurements.

Figure 3: Synergistic Wnt PCP activation by Wnt8a and Ror2 in zebrafish and Xenopus embryos. (A) Embryos at 11 hpf were fixed and subjected to *in situ* hybridization against *hgg/ntl*. Scale bar represents 200µm. (B) Embryos were sorted according to their phenotypes into groups (see Supplementary Figure 2 for details). (C) *gsc:memGFP* embryos were microinjected with indicated constructs, fixed at 11 hpf and a defined z-stack was imaged by confocal microscopy. Confocal stack shows the notochord marked by *gsc:memGFP* from a dorsal view with animal site to the top. Magnified inset highlights the shape of notochord cells. Scale bar represents 20µm. (D) Analysis of cell roundness. Boxplot shows the width/length ratio of 25 notochordal cells. Circularity ranges from 0 (infinitely elongated polygon) to 1 (perfect circle). ANOVA confirmed that cell roundness is significantly different in the analyzed groups with a $P= 2.91*10^{-24}$, confidence interval 95%, F value=37, and df=149. (E) ATF luciferase reporter assay of pooled Xenopus gastrulae injected with indicated constructs and the ATF2 firefly and Renilla luciferase reporter. E shows the mean with S.D. of three independent experiments. ***=P<0.001, **=P<0.01, *=P<0.05.

Figure 4: In-depth analysis and simulation of Wnt-positive cytonemes in zebrafish embryos *in vivo* (A) Live confocal microscopy analysis for filopodia dynamics over time. Mosaic expression of memCherry was utilized to quantify the protrusions of single cells at positions as indicated. The image shows the same cells at different times during zebrafish gastrulation. (B) Filopodia of cells in A were measured by a semi-quantitative segmentation software (see Supplementary Figure

4 for details). Quantification illustrates the mean filopodia length and number per cell with SEM at different time points. (C) Effect of Ror2 on filopodia length/number. Live confocal microscopy analysis for filopodia of embryos injected with Ror2 or $Ror2^{3I}$ mRNA at one cell stage. (D) Diagram of mean filopodia length and number per cell with SEM. (E) Analysis of Wnt cytonemes during live imaging. Embryos were microinjected at 16 cell stage to generate a cell clone expressing Wnt8a-GFP and memCherry to visualize cytonemes and Ror2, $Ror2^{3I}$ or Ror2-MO oligomer. Confocal images were taken of single cells and subjected to filopodia length/number measurement. See Suppl. Fig. 4 for stacked diagrams with chi-squared test analysis. (F) Bar diagram shows number of filopodia without Wnt8a-GFP (i.e. GFP signal below detection limit) or filopodia carrying Wnt8a-GFP (cytonemes) (i.e. GFP signal above detection limit) per cell. Statistical analysis ***=P<0.001, **=P<0.01, =P<0.05. Data meet the assumption (B) that filopodia length and number are significantly different at the analyzed time-points (One-way ANOVA, $P=1.35*10^{-9}$, confidence interval 95%, F value=27.6, and df=73) and (D) that the filopodia number and length are significantly different across treatments ($P=1.61542*10^{-7}$, confidence interval 95%, F value=24.6, and df=39). (G) Simulation of Wnt dissemination in a growing tissue over 180min. Wnt8a is distributed in a graded manner in the target tissue. Modeling the dynamically expanding tissue with single cell resolution and discrete implementation of cytoneme-based transport establishes a morphogen gradient over the length of the developing tissue. Based on the cytoneme appearance measured in (D & F), Ror2 activity in the Wnt producing cells alters the input of Wnt in the target field which is directly incorporated into the simulation by altering the formation frequency of cytonemes and thus ligand concentration in the neighboring tissue. Simulated time in minutes after the onset of Wnt production at 4hpf.

Figure 5: Visualization of Ror2-Wnt8a cytonemal transport and Lrp6 receptor clustering in the living zebrafish . (A) Illustration of the injection procedure to generate single cell clones. (B-C) Time series of a single confocal plane of Ror2-mCherry/Wnt8a-GFP expressing cells to (B) observe Wnt8a recruitment to the membrane and cytoneme initiation and (C) cytonemal target finding and Ror2/Wnt8a cluster endocytosis into the receiving cell. Optimal microscopical settings were used to allow an improved axial resolution of ca. 250nm. Single channels in Suppl. Fig 5A and B and movie in Suppl. Movie 3. White arrows indicate the Wnt8a/Ror2 cluster while the yellow arrow highlights pruning of the cytoneme tip after successful

cytonemal delivery. Yellow arrows mark the Wnt8a/Ror2 cluster. (D) Wnt8a-mCherry cytoneme leads to Lrp6-GFP accumulation and co-localization at the receiving cell. (E) Illustration of the injection procedure to generate clones to visualize paracrine signal transport. (E) 3D-stack of a Wnt8a-mCherry cytoneme leading to Lrp6-GFP accumulation and co-localization at the receiving cell. Close-up shows a single plane including orthogonal YZ and XZ views of the cytoneme contact point. (F) Single plane image of a Ror2-mCherry/Wnt8a cell leading to Lrp6-GFP clustering on cytoneme contact site. Scale bars = 10 µm; in E = 20 µm.

Figure 6: Ror2 enhances paracrine Wnt/β-catenin signaling in zebrafish embryos and HEK293T co-culture. (A) Microinjected embryos at indicated stages were fixed and subjected to *in situ* hybridization against the Wnt target gene (*axin2*) or markers for brain patterning (*fgf8a, pax6a*). Brackets indicate expansion of Wnt target gene expression (*axin2*), distance of fgf8 expression domains or forebrain territory (*pax6a*), while the asterisk indicates a lack of forebrain tissue. (B) Co-culture reporter gene assay in HEK293T cells. TCF/Wnt reporter population was transfected with 7xTRE Super TOPFlash-NLS-mCherry and Lrp6 and co-cultured with a second population as indicated. Co-culture principle can be seen in Supplementary Figure 6. (C) Relative reporter activation by measuring the mCherry signal. Bar diagram represents the mean value with SEM of 3 independent experiments. Scale bar represents 200µm. (D) RT-qPCR-based expression assay in zebrafish embryos. Embryos were injected at 16 cell stage to generate a distinct signaling center at 75% epiboly (see Supplementary Figure 6 for details) and were subjected for RTqPCR. Relative ΔΔCt expression values of Wnt-β-catenin target genes *axin2* and *lef1* is acquired by normalization to actb1 and in comparison to a control-injected sample (relative ctrl expression level shown as a dotted line). Each condition represents the mean Rt-qPCR result of 4 x 50 embryos acquired from 2 independent experiments. ***=P<0.001, *=P<0.05. ANOVA confirmed hypothesis that expression levels are different between treatments with a P= 0.00025, confidence interval 95%, F value 33.9, df 11.

Figure 7: Importance of ror2 dependent cytonemes in gastric cancer cell proliferation and intestinal crypt cells organoid formation. (A) Confocal Z-projection of live AGS cells transfected with memGFP and Wnt8a-mCherry. Yellow arrow marks a cytoneme and yellow outlined arrow highlights circular Wnt8a-mCherry spots around the source cell. (B) Confocal Z-projection of fixed AGS cells

transfected with Ror2-mCherry and stained with LifeAct. Yellow arrow marks filopodia connections to adjacent cells and yellow outlined arrow highlights Ror2-mCherry clusters in a non-transfected adjacent cell. (C) Boxplot of cumulative filopodia lengths for AGS cells transfected with an empty plasmid, Ror2 or Ror2^{3l}. (D, E) Proliferation assay of nucRFP transfected AGS cells after a 48 hrs co-cultivation with cells transfected with indicated constructs. D shows fluorescent images which were subjected for cell counting. Average nucRFP cells per image are shown in Boxplot E. (F) Fluorescent images of purified intestinal myofibroblasts transfected with control siRNA (n=31) or Ror2 siRNA (n=29) were quantified for cumulative filopodia length per cell. (G) Boxplot of number of formed organoids of PORCN deficient intestinal crypt cells co-cultured with indicated cell population for 3-4 days. Organoid numbers were normalized to crypt cells transfected with ctrl siRNA. ***=P<0.001, **=P<0.01, *=P<0.05. One-way ANOVA confirmed significant differences between treatments with a confidence interval 95% in (C) P= $3.6151*10^{-7}$, F value 16.8, df 122; in (D) P = $6.67274*10^{-5}$, F value 9.4, df 46; (in F) P = $3.32078\ 10^{-06}$, F value 26.5 , df 59; and in (G) P = $1.42034*10^{-18}$, F value 106.9 , df 41.

Material and Methods

Plasmids. The following plasmids have been used: pCS2+zfWnt8aORF1 (Addgene 17048), pCS2+zfWnt8aORF1-GFP , pCS2+zfWnt8aORF1-mCherry (Stanganello et al., 2015), pCS2+xWnt5a-GFP, pCS2+zfWnt5b (Wallkamm et al., 2014), xRor2-mCherry (Feike et al., 2010), xRor2^{3I} (Casella et al., 1981), mRor2-dCRD-GFP, pCS2+Fz7a-CFP , pcDNA3-EGFP-Cdc42T17N (Addgene 12976), 7xTRE Super TOPFlash-NLS-mCherry (Moro et al., 2012), pmKate2-f-mem (Evrogen), GPI-anchored mCherry in pCS2+ (Scholpp et al., 2009), IRSp53^{4K} (Casella et al., 1981). To generate the pCS2+xRor2 construct, the open reading frame of xRor2-mCherry was inserted in the ClaI/XhoI site of pCS2+.

Maintenance of fish. Breeding zebrafish (*Danio rerio*) were maintained at 28°C on a 14 h light/10 h dark cycle (Brand et al., 2002). To prevent pigment formation, embryos were raised in 0.2 mM 1-phenyl-2-thiourea (PTU, Sigma, St Louis, MO 63103 USA) after 24 hpf. The data we present in this study were acquired with wild-type zebrafish (AB2O2) as well as with the transgenic zebrafish line tg(-6gsc:EGFP-CAAX) (Smutny et al., 2017). All animal work (zebrafish husbandry and experimental procedures) were undertaken under project and personnel licences granted by the UK Home Office under the United Kingdom Animals (Scientific Procedures) Act, in accordance with The University of Exeter's ethical policies and approved by the University of Exeter's Animal Welfare and Ethical Review Body, and in accordance with the German law on Animal Protection approved by Local Animal-Protection Committee (Regierungspräsidium Karlsruhe, Az.35-9185.64) and the Karlsruhe Institute of Technology (KIT).

Cell culture experiments. Experiments were performed in zebrafish PAC2 fibroblasts derived from 24 h old zebrafish embryos cultivated at 28°C without additional CO_2 supply, primary gastric adenocarcinoma cells (AGS), Gastric tubular adenocarcinoma liver metastasis cells (MKN28, MKN7 (Motoyama et al., 1986)) and human embryonic kidney cells (HEK293T; CRL-1573) cultivated at 37°C with 5% additional CO_2 supply. PAC2 were maintained in Leibowitz-15 media, HEK in DMEM, AGS and MKN28 in RPMI 1640, all supplemented with 10% fetal bovine serum, 1%

L-Glutamine (2 mM) and 1% Penicillin/Streptomycin. All the material used for cell culture was purchased from Life Technologies, Gibco.

For transfection experiments FuGENE HD Transfection Reagent (Promega) was used and cells were imaged after 48 hrs. For co-culture experiments, transfected cells were incubated for 24 hrs, detached by Trypsin-EDTA (0.05%) and incubated in a mixed population for another 48 hrs before image acquisition.

Assays for SuperTOPFlash (STF) TCF/Wnt reporter expression and proliferation required initial co-cultivation of two distinct cell populations. Cells were transfected with pDest7xTCF-NLS-mCherry or pCS2+nucRFP plasmids, respectively, and incubated for 24 hrs, detached by Trypsin-EDTA (0.05%) and further incubated in a mixed population for another 72 hrs before image acquisition. For one replication seven 10x magnification images were taken per sample with identical laser settings. Image locations were saved by the Mark&Find microscope feature to reproduce similar scanning setups. For measuring TCF/Wnt reporter activation, fluorescent nuclei were processed using the Dot-Plugin in Imaris and the average grey value of the nuclei was determined or fluorescent nuclei were counted to measure cell proliferation.

For the chemical treatment, cell cultures were treated with GTPase Inhibitor ML141 10 mM (Merck Millipore) or 50 µM IWR-1 (Sigma) to antagonise the Wnt signaling pathway. For staining, cells were fixed with 4% PFA at RT, washed with PBS. Cells were incubated with 50 µg/ml phalloidin (P1951, Sigma) and 10 µg/ml DAPI (D9542, Sigma).

Organoid formation of intestinal crypt cells. Myofibroblasts were prepared from C57BL/6-*Tg(Pdgfra-cre)1Clc/J /Rosa*^{mTmG} mice and cultured as previously described (Greicius et al., 2018). As confluence of cultured cells was reaching 80%, they were transfected with respective siRNA (Dharmacon mouse ROR2 siRNA pool Cat#LQ-041074-00-0002, four siRNAs combined in equal parts at 10nM) using siRNAmax reagent (Invitrogen Cat#13778-030). On day 2 post-transfection, myofibroblasts were mixed with *Porcn* deficient intestinal epithelial cells and cultured using RSPO1 supplemented medium. Organoid counting was performed at the time point when group containing no stromal cells had no surviving organoids left (end of day 3- beginning of day 4 of co-culture). siRNA transfected cells were imaged using OlympusLive Imaging system IX83. Acquired 3D image stacks were de-convoluted

using cellSens Dimension (Olympus) and are presented as maximum intensity projections.

Automated filopodia analysis software. Cells and their attached filopodia were automatically detected in the RFP channel (mem-mCherry) of the acquired images (Suppl. Fig. 4A). The images were initially filtered using a Gaussian low-pass filter ($\sigma^2 = 1$) and subsequently used detect the cell body as well as the cell's filopodia (Suppl. Fig. 4B). For the filopodia detection we used an objectness filter ($\sigma = 1, \alpha = 1, \beta = 1, \gamma = 0.003, N = 2$) that emphasized line-like structures based on the eigenvalues of the Hessian matrix at each pixel location (Suppl. Fig. 4C (Antiga, 2007). The obtained edge-enhanced image was then binarized (Suppl. Fig. 4D) using a local adaptive threshold filter that set pixels to foreground if their intensity value was larger than a regional mean intensity minus a multiple of the regional intensity standard deviation and otherwise to background (window radius = 200, std. dev. multiplier = 1). To segment the cell body, we applied the local adaptive threshold (window radius = 200, std. dev. multiplier = 1) on the smoothed input image (Suppl. Fig. 4E) and subsequently used a morphological opening operation (kernel radius = 2) to get rid of noise and remaining filopodia parts (Suppl. Fig. 4F (Soille et al., 2011)). The cell body was given by the largest connected component in the opened binary image. The segmentation mask of the cell body including filopodia was then constructed by combining the binarized edge-enhanced image with the binary cell body image (Suppl. Fig. 4G). The combined cell image was subsequently skeletonized to identify potential filopodia tips at the end points of the skeleton (Suppl. Fig. 4H). All above-mentioned preprocessing steps were implemented in the open-source software tool XPIWIT (Bartschat et al., 2016).

The preprocessing results were then imported to a dedicated MATLAB tool that was developed to validate, correct and analyze this kind of images (Suppl. Fig. 4I, J). In order to automatically trace filopodia from the identified tips to the cell body, we used an adapted livewire algorithm (Barrett and Mortensen, 1997). The output of the objectness filter was used as an edge map (Suppl. Fig. 4C) on which the livewire algorithm tried to find a maximally scoring path from the tip of the filopodium to the center of the cell body. Based on the segmentation of the cell body (Suppl. Fig. 4F), the automatic tracing was stopped as soon as the cell body was reached. The interactive user interface was then used to add, remove and correct both

segmentation masks and detected filopodia on a per-cell basis. For each cell's filopodia, we calculated the Euclidean distance along the the path from the tip to the cell body. The same image preprocessing and tracing was applied to semi-automatically extract filopodia in 3D confocal images (Suppl. Fig. 4K). However, for the 3D case, start and end points of the filopodia were provided by the user via a graphical user interface and the livewire approach was applied twice. First on an axial maximum intensity projection (z) to obtain the lateral path (xy). Subsequently, the axial positioning of the filopodium was obtained by searching for the highest scoring path between the provided start and end points solely in the z-direction (Suppl. Fig. 4K). Multiple automatically traced filopodia can then be exported and used to obtain average statistics of all filopodia of interest.

IsFCS. For the FCS measurements, a home-built confocal microscope was used as previously described (Dörlich et al., 2015), with slight modifications. We used a water immersion objective (HCX PL APO CS 63x /1.2, Leica, Wetzlar, Germany) instead of an oil immersion objective; the multimode fiber, which acts as a confocal pinhole, was modified accordingly to ensure a pinhole size of 1 AU. Data were collected for 390 s by continuously scanning the focus perpendicularly through the membrane. Each scan line consisted of 100 pixels, with a step size of 100 nm. eGFP was excited with a 488 nm continuous wave (cw) laser and mCherry with a 561 nm cw laser. After splitting the fluorescence signal into two color channels by using a 555 nm dichroic filter, 525/50 (eGFP) and 600/37 (mCherry) band pass filters were used for detection. To avoid artefacts in the correlation curves caused by scanner flyback and wavelength switching, the membrane was always kept in the center of the field of view. The intensity data were arranged as an *x-t* pseudo image, and the intensities of those pixels containing membrane fluorescence were integrated to obtain an intensity time trace for correlation analysis, as described earlier (Hunter, 2007).

Functional analysis. The injection of mRNAs and Morpholino oligomers were performed according to the description in the text and in (Mattes et al., 2012). Ror2 MO was used in a 0.5mM concentration (5'-CAGTGTAACAACTTCCAAACTCTCC -3') (Gene Tools, Philomath, OR 97370 USA). Capped and *in vitro* transcribed mRNA, (mMessage Machine Kit, Ambion) was microinjected into one cell or into the yolk for ubiquitous expression or in one of 16 blastomeres to generate cell clones. Embryos

were incubated at 28°C until subjected for image acquisition or fixed for whole-mount mRNA *in situ* hybridization (ISH).

For *in situ* hybridization, *hgg*, *ntl*, *axin2*, *fgf8a* and *pax6a* digoxigenin- and fluorescein-labeled probes were prepared from linearized templates using an RNA labelling and detection kit (Roche) as described in (Scholpp and Brand, 2003). Images were taken on an Olympus SZX16 microscope equipped with a DP71 digital camera by using Cell D imaging software.

For real-time quantitative PCR (RT-qPCR), 50 embryos each were lysed in 1 ml TriZol (Sigma), and total RNA was prepared using Direct-zol RNA Mini Prep Kit from Zymo Research. cDNA was prepared using MMLV reverse transcriptase from Promega and analysed in a Real-Time PCR system from LifeTechnologies (ABI StepOnePlus). Primers with the following sequence were used: *beta-actin* (5´-CCTTCCTTCCTGGGTATGG-3´; 5´-GGTCCTTACGGATGTCCAC-3´), *axin2* (5´-CAATGGACGAAAGGAAAGATCC-3´; 5´-AGAAGTACGTGACTACCGTC-3´), *lef1* (5´-CAGACATTCCCAATTTCTATCC-3´; 5´-TGTGATGTGAGAACCA ACC-3´). Results were analysed using the ΔΔCT method.

Simulations. Computer simulations have been implemented in Python using the libraries numpy, scipy and matplotlib (Hunter, 2007) and is based on a simulation of cytoneme-based ligand distribution described in detail in (Stanganello et al., 2015).The modelling of the tissue is split up into two subproblems (1) the correct modelling of the dynamically forming tissue and (2) the morphogen transport through that tissue. The tissue dynamics are modelled by a two-dimensional non-periodic plane of discrete cells. The simulated area is 1000 by 1000 µm in size and each cell occupies a circle of 8µm radius. Possible cell positions are precomputed and kept fixed during the course of the simulation. Cells can change positions by moving along those precomputed positions. In every simulation step (Δt=1 s) each individual cell has the possibility to perform some actions with predetermined probabilities which are directly derived from experimental measurements.

Possible actions are (i) Signaling from the producing tissue, (ii) Cell insertion by division or intercalation of the receiving tissue, (iii) Cell migration - directed or non-directed nearest neighbor swapping of the receiving tissue, and (iv) Morphogen decay in the receiving tissue. Two different cell types are distinguished. The marginal, Wnt active cells are producing morphogen and are able to deposit

morphogen via cytonemes to cells of the receiving tissue. Once a signaling event is accepted for a marginal cell an angle is randomly chosen from the respective distribution determined in (Stanganello et al., 2015). The length is randomly chosen from a Gaussian distribution with the peak value l_{filo}. A virtual filopodium is formed with those values originating from the marginal cell. If the tip of the filopodium ends up in vicinity of the surface of a receiving cell (±2µm) the Wnt content of that cell is increased, otherwise the filopodium is deleted. Probabilities used in the simulation were:

	Signaling probability p_{filo}
WT	$\frac{1}{30}$
Ror2	$1.61 \cdot \frac{1}{30} = 0.0537$
Ror2^{3I}	$0.338 \cdot \frac{1}{30} = 0.0113$

Tissue expansion during neural plate patterning is driven by the intercalation of cell layers during the thinning out of the cell sheet as well as cell division. Since we are only modelling one cell layer both of these processes can be incorporated by a single action, namely cell insertions. If a cell insertion event is accepted in a receiving cell a path to the nearest empty grid spot is obtained and all cells are subsequently moved along that path. The emerging empty grid spot is then filled with a randomly chosen cell with the same distance ±6µm from the marginal cells. To include the highly dynamic intermingling of the cells during that process an additional action, cell migration, is added. This action allows for a cell to swap places with a randomly chosen nearest neighbor cell. Morphogen decay inside the receiving tissue is implemented by an action that decreases the Wnt content of the cell once accepted.

Luciferase reporter assay in Xenopus embryos. For the ATF2 luciferase reporter assay, 4-cell stage Xenopus embryos were injected into both animal ventral blastomeres with the 100 pg ATF2-Luciferase reporter plasmid in combination with 10 pg TK-Renilla-Luciferase reporter plasmid. The reporter plasmids were injected alone or together with 500 pg of the respective synthetic mRNAs. Luciferase reporter assays were carried out from triplicates of five gastrula stage (st.12) embryos lysed to measure Luciferase activity using the Dual luciferase system (Promega).

Image acquisition. For confocal analysis, live embryos were embedded in 0.7% low melting agarose (Sigma-Aldrich) dissolved in 1x Ringer's solution. Images of cells and embryos were obtained with a Leica TCS SP5 X or SP8X confocal laser-scanning microscope using 20x or 63x dip-in objective or for the kinase library screen a Leica DMI600SD with 20x objective was used. Image processing was performed with Imaris 9.1 software (Bitplane AG, Switzerland). Filopodia and cytoneme measurements from confocal z-Stacks of living embryos was performed via the semi-automated filopodia analysis software described before. Cell culture quantifications were carried out by using Fiji software. Roundness of notochordal embryo cells was determined by calculating the width to length ratio per cell in Fiji.

Statistical analysis. All experiments were carried out at least in biological triplicates if not indicated otherwise. Significance was calculated by Student's t-test while asterisks represent indicated p-values. One-way ANOVA was used to analyse groups of experimental data. All groups are random samples from the same population. Variances are similar across treatments and residuals are normally distributed. P-values, F values and degrees of freedom (df) are indicated. Box plots: Centre lines show the medians; box limits indicate the 25th and 75th percentiles as determined by R software; whiskers extend 1.5 times the interquartile range from the 25th and 75th percentiles, outliers are represented by dots.

Supplementary figure legends

Supplementary Figure 1: (A-B) Bar diagram shows the average lengths (A) or numbers (B) of filopodia per PAC2 cell. Error bar represents the SEM.

Supplementary Figure 2: (A) 3D confocal image of a cell clone at 50% epiboly. Embryo was injected with memCherry and Wnt8a-GFP. Cytonemes feature Wnt8a-GFP clusters on their tip (arrows). (B) Single confocal planes of embryos injected with Wnt5b-GFP and memCherry or Ror2-mCherry. (C) Intensity profiles along 15 µm of cell membrane containing Wnt5b-GFP spots, showing spatial intensity correlations with Ror2-mCherry. (D) Schematic depiction of the principle of line scanning FCS measurements, which allows us to remove fluorescence fluctuations due to membrane motion. Red and green emitting laser foci are scanned perpendicularly through the plasma membrane. The emission is recorded as a function of time and corrected for membrane fluctuations. The autocorrelation functions of Ror2-mCherry (red excitation) and Wnt8a-GFP (green excitation) are computed from the intensity time traces and yield local concentrations (i.e., area densities) and diffusional correlation times. The cross-correlation between red and green is a measure of joint intensity fluctuations in the two channels caused by Wnt8a-GFP bound to Ror2-mCherry diffusing together through the excitation focus. (E) Diagram of confocal planes of embryos injected with Wnt8a-GFP, Ror2-mCherry and Fzd7a-CFP and the corresponding intensity correlation. (F, G) Pearson correlation coefficients of pairs of fluorescent proteins in a dual-color image (as indicated by the black boxes below the bar graph). The result is +1 for perfect correlation, 0 for no correlation. (F) shows the analysis of confocal images of embryos at 50% epiboly injected with the indicated constructs, as determined by Imaris software. (G) shows a Pearson co-localization analysis of indicated fluorescent constructs in a tissue volume of 40 x 40 x 60 μm^3 of 8 different embryos. *** = $P < 0.001$.

Supplementary Figure 3: (A) Microinjection of Ror2-mCherry mRNA in rising concentrations and classification of phenotypes into groups showing developmental alterations at 24 hpf. Chi-squared test was performed to determine p-values. (B) Classification of embryos into 3 groups of phenotypes depending on their *ntl*

expression. (C) Quantification of the ntl expression width. Location of measurement is shown in the left image (dorsal view, animal to the top) and the bar diagram represents average width with SEM. ***=P<0.001, *=P<0.05.

Supplementary Figure 4: Cytoneme quantification software to automatically extract filopodia using the memCherry channel of the acquired images. The raw image (A) was initially smoothed with a Gaussian low-pass filter (B) to reduce image noise for facilitated processing. To emphasize filopodia in the image, we used an objectness filter that emphasizes line-like structures based on the eigenvalues of the Hessian matrix (C) and binarized the resulting edge image (D) using local adaptive thresholding. For the detection of the cell body, we applied a local adaptive threshold to the Gaussian smoothed raw image (E) and performed a morphological opening operation to remove filopodia remains from the cell body (F). The two binarized images (D) and (F) were then combined to yield the final segmentation mask including cell body and filopodia (G). Finally, the combined binary image (G) was used to obtain a skeleton image (H), which in turn allows extracting potential filopodia tips at the end points of the skeleton. The identified cell body (cyan outline) and the potential filopodia tips (magenta dots) are shown in (I). A livewire approach was then used to automatically trace filopodia from the tips to the cell body (J, red lines). The white arrow indicates errors of the automatic tracing and a dedicated software can be used to manually correct such errors. (K) To measure analyse filopodia in acquired 3D images, we developed custom-made MATLAB GUI that allows to scroll through the slices of the stack and to semi-automatically trace filopodia based on manually provided start and end points of a filopodium of interest (yellow arrows). The software automatically traces the filopodium in 3D using a livewire approach to obtain accurate length quantifications. The software keeps track of all segmented filopodia, provides filopodia counts, length measurements as well as average quantifications of all identified filopodia. In addition, in a window of the GFP channel we are able to distinguish between Wnt positive and Wnt negative filopodia for embryos expressing Wnt8a-GFP.

Supplementary Figure 5: Visualization of Ror2-Wnt8a cytonemal transport in the living zebrafish. Time series of still pictures of single channels of Ror2-mCherry/Wnt8a-GFP expressing cells to (A) observe Wnt8a recruitment to the

membrane and cytoneme initiation and (B) cytonemal target finding and Ror2/Wnt8a cluster endocytosis into the receiving cell. White arrows indicate the Wnt8a/Ror2 cluster while the yellow arrow highlights pruning of the cytoneme tip after successful cytonemal delivery. (B) includes also a series of merged pictures with the bright field channel. Scale bars = 10 µm; in E = 20 µm.

Supplementary Figure 6: (A) Illustration of expression domains of landmark genes e.g. *axin2*, *fgf8* or *pax6a*. (B) Illustration of the experimental procedure for *in vitro* co-cultivation assays with HEK293T cells expressing cytoneme regulators and the TCF/Wnt reporter 7xTRE SuperTOPFlash-NLS-mCherry. Fluorescence image shows some activated cells expressing nuclear mCherry. All cells were fixed and stained with DAPI. (C) Workflow of clonal injection to induce a local Wnt source with following RTqPCR analysis of target genes in responding cells.

Supplementary Figure 7: (A) Confocal images of gastric cancer cells AGS, MKN7 and MKN28. Cells were transfected with Wnt8a-mCherry (left) or Ror2mCherry (right), fixed and stained with LifeAct. Yellow Arrows highlight Wnt8a-mCherry cytonemes or Ror2-induced protrusions while yellow outlined arrows visualize the dissemination of Wnt8a-mCherry clusters to untransfected adjacent cells. (B) Illustration of the experimental procedure in co-cultivation assays to determine the proliferation of a second cell population. (C) Mouse crypt organoid supported by a purified intestinal myofibroblasts derived from a PdgfRα-Cre driven GFP reporter mouse. Image was taken 3 days after co-culture of myofibroblasts with *Porcn* deficient intestinal epithelial cells. Long cell protrusions surrounding the organoid are highlighted by yellow arrows.

Supplementary movie legends

Supplementary Movie 1: Time-lapse movie of localization of Ror2-mCherry and Wnt8a-GFP in a developing zebrafish embryo at gastrulation stages. Movie illustrates the co-localization of Ror2-mCherry and Wnt8a-GFP in clusters and their dynamics over time. Single confocal plane was imaged at 6 hpf for 20 minutes with a frame rate of 15 seconds. Still pictures of the movie in Fig. 2A.

Supplementary Movie 2: Time-lapse movie of clonal cells forming cytonemes in a developing zebrafish embryo at gastrulation stages. Z-projection of a clone of Wnt8a-GFP and Ror2-mCherry positive cells was imaged at 8 hpf for 20 minutes with a frame rate of 15 seconds.

Supplementary Movie 3: Time-lapse movie of clonal cells forming cytonemes in a developing zebrafish embryo at gastrulation stages. Single confocal plane of a clone of Wnt8a-GFP and Ror2-mCherry positive cells showing cytonemal target finding and subsequent Ror2/Wnt8a cluster endocytosis of the receiving cell. Movie was imaged at 8 hpf for 20 minutes with a frame rate of 15 seconds. Still pictures of the movie in Fig. 5C and single channels are presented in Suppl. Figure 5B.

References

Alexandre, C., Baena-Lopez, A. and Vincent, J.-P. (2014). Patterning and growth control by membrane-tethered Wingless. *Nature* **505**, 180–185.

Anastas, J. N. and Moon, R. T. (2013). WNT signalling pathways as therapeutic targets in cancer. *Nat. Rev. Cancer* **13**, 11–26.

Andre, P., Song, H., Kim, W., Kispert, A. and Yang, Y. (2015). Wnt5a and Wnt11 regulate mammalian anterior-posterior axis elongation. *Development* **142**, 1516–1527.

Antiga, L. (2007). Generalizing vesselness with respect to dimensionality and shape. *insight-journal.org*

Aoki, R., Shoshkes-Carmel, M., Gao, N., Shin, S., May, C. L., Golson, M. L., Zahm, A. M., Ray, M., Wiser, C. L., Wright, C. V. E., et al. (2016). Foxl1-expressing mesenchymal cells constitute the intestinal stem cell niche. *Cell Mol Gastroenterol Hepatol* **2**, 175–188.

Bai, Y., Tan, X., Zhang, H., Liu, C., Zhao, B., Li, Y., Lu, L., Liu, Y. and Zhou, J. (2014). Ror2 receptor mediates Wnt11 ligand signaling and affects convergence and extension movements in zebrafish. *Journal of Biological Chemistry* **289**, 20664–20676.

Barrett, W. A. and Mortensen, E. N. (1997). Interactive live-wire boundary extraction. *Medical Image Analysis* **1**, 331–341.

Bartschat, A., Hübner, E., Reischl, M., Mikut, R. and Stegmaier, J. (2016). XPIWIT--an XML pipeline wrapper for the Insight Toolkit. *Bioinformatics* **32**, 315–317.

Bartscherer, K. and Boutros, M. (2008). Regulation of Wnt protein secretion and its role in gradient formation. *EMBO Rep.* **9**, 977–982.

Bänziger, C., Soldini, D., Schütt, C., Zipperlen, P., Hausmann, G. and Basler, K. (2006). Wntless, a conserved membrane protein dedicated to the secretion of Wnt proteins from signaling cells. *Cell* **125**, 509–522.

Beckett, K., Monier, S., Palmer, L., Alexandre, C., Green, H., Bonneil, E., Raposo, G., Thibault, P., Le Borgne, R. and Vincent, J.-P. (2013). Drosophila S2 cells secrete wingless on exosome-like vesicles but the wingless gradient forms independently of exosomes. *Traffic* **14**, 82–96.

Beumer, J. and Clevers, H. (2016). Regulation and plasticity of intestinal stem cells during homeostasis and regeneration. *Development* **143**, 3639–3649.

Billiard, J., Way, D. S., Seestaller-Wehr, L. M., Moran, R. A., Mangine, A. and Bodine, P. V. N. (2005). The orphan receptor tyrosine kinase Ror2 modulates canonical Wnt signaling in osteoblastic cells. *Mol. Endocrinol.* **19**, 90–101.

Brand, M., Granato, M. and Nüsslein-Volhard, C. (2002). *Keeping and Raising Zebrafish*. (eds. Nüsslein-Volhard, C. and Dahm, R. Oxford University Press.

Brinkmann, E.-M., Mattes, B., Kumar, R., Hagemann, A. I. H., Gradl, D., Scholpp, S., Steinbeisser, H., Kaufmann, L. T. and Özbek, S. (2016). Secreted Frizzled-related Protein 2 (sFRP2) Redirects Non-canonical Wnt Signaling from Fz7 to Ror2 during Vertebrate Gastrulation. *Journal of Biological Chemistry* **291**, 13730–13742.

Casella, J. F., Flanagan, M. D. and Lin, S. (1981). Cytochalasin D inhibits actin polymerization and induces depolymerization of actin filaments formed during platelet shape change. *Nature* **293**, 302–305.

Chen, Q., Su, Y., Wesslowski, J., Hagemann, A. I., Ramialison, M., Wittbrodt, J., Scholpp, S. and Davidson, G. (2014). Tyrosine phosphorylation of LRP6 by Src and Fer inhibits Wnt/β-catenin signalling. *EMBO Rep.* **15**, 1254–1267.

Chiurillo, M. A. (2015). Role of the Wnt/β-catenin pathway in gastric cancer: An in-depth literature review. *World J Exp Med* **5**, 84–102.

Disanza, A., Bisi, S., Winterhoff, M., Milanesi, F., Ushakov, D. S., Kast, D., Marighetti, P., Romet-Lemonne, G., Müller, H.-M., Nickel, W., et al. (2013). CDC42 switches IRSp53 from inhibition of actin growth to elongation by clustering of VASP. *The EMBO Journal* **32**, 2735–2750.

Dörlich, R. M., Chen, Q., Niklas Hedde, P., Schuster, V., Hippler, M., Wesslowski, J., Davidson, G. and Nienhaus, G. U. (2015). Dual-color dual-focus line-scanning FCS for quantitative analysis of receptor-ligand interactions in living specimens. *Sci Rep* **5**, 10149.

Farin, H. F., Jordens, I., Mosa, M. H., Basak, O., Korving, J., Tauriello, D. V. F., de Punder, K., Angers, S., Peters, P. J., Maurice, M. M., et al. (2016). Visualization of a short-range Wnt gradient in the intestinal stem-cell niche. *Nature* **530**, 340–343.

Feike, A. C., Rachor, K., Gentzel, M. and Schambony, A. (2010). Wnt5a/Ror2-induced upregulation of xPAPC requires xShcA. *Biochem. Biophys. Res. Commun.* **400**, 500–506.

Glickman, N. S., Kimmel, C. B., Jones, M. A. and Adams, R. J. (2003). Shaping the zebrafish notochord. *Development* **130**, 873–887.

Gradilla, A.-C. and Guerrero, I. (2013). Cytoneme-mediated cell-to-cell signaling during development. *Cell Tissue Res* **352**, 59–66.

Green, J. L., Inoue, T. and Sternberg, P. W. (2007). The C. elegans ROR receptor tyrosine kinase, CAM-1, non-autonomously inhibits the Wnt pathway. *Development* **134**, 4053–4062.

Greicius, G., Kabiri, Z., Sigmundsson, K., Liang, C., Bunte, R., Singh, M. K. and Virshup, D. M. (2018). PDGFRα+ pericryptal stromal cells are the critical source of Wnts and RSPO3 for murine intestinal stem cells in vivo. *Proc. Natl. Acad. Sci. U.S.A.* **115**, E3173–E3181.

Gross, J. C., Chaudhary, V., Bartscherer, K. and Boutros, M. (2012). Active Wnt proteins are secreted on exosomes. *Nat Cell Biol* **14**, 1036–1045.

Grumolato, L., Liu, G., Mong, P., Mudbhary, R., Biswas, R., Arroyave, R., Vijayakumar, S., Economides, A. N. and Aaronson, S. A. (2010). Canonical and noncanonical Wnts use a common mechanism to activate completely unrelated coreceptors. *Genes Dev* **24**, 2517–2530.

Hagemann, A. I. H., Kurz, J., Kauffeld, S., Chen, Q., Reeves, P. M., Weber, S., Schindler, S., Davidson, G., Kirchhausen, T. and Scholpp, S. (2014). In vivo analysis of formation and endocytosis of the Wnt/β-Catenin signaling complex in zebrafish embryos. *J Cell Sci* **127**, 3970–3982.

Hikasa, H., Shibata, M., Hiratani, I. and Taira, M. (2002). The Xenopus receptor tyrosine kinase Xror2 modulates morphogenetic movements of the axial mesoderm and neuroectoderm via Wnt signaling. *Development* **129**, 5227–5239.

Ho, H.-Y. H., Susman, M. W., Bikoff, J. B., Ryu, Y. K., Jonas, A. M., Hu, L., Kuruvilla, R. and Greenberg, M. E. (2012). Wnt5a-Ror-Dishevelled signaling constitutes a core developmental pathway that controls tissue morphogenesis. *Proc. Natl. Acad. Sci. U.S.A.* **109**, 4044–4051.

Holzer, T., Liffers, K., Rahm, K., Trageser, B., Özbek, S. and Gradl, D. (2012). Live imaging of active fluorophore labelled Wnt proteins. *FEBS Lett.* **586**, 1638–1644.

Huang, H. and Kornberg, T. B. (2016). Cells must express components of the planar cell polarity system and extracellular matrix to support cytonemes. *Elife* **5**, 197.

Hunter, J. D. (2007). Matplotlib: A 2D Graphics Environment. *Comput. Sci. Eng.* **9**, 90–95.

Kabiri, Z., Greicius, G., Madan, B., Biechele, S., Zhong, Z., Zaribafzadeh, H., Edison, Aliyev, J., Wu, Y., Bunte, R., et al. (2014). Stroma provides an intestinal stem cell niche in the absence of epithelial Wnts. *Development* **141**, 2206–2215.

Kast, D. J., Yang, C., Disanza, A., Boczkowska, M., Madasu, Y., Scita, G., Svitkina, T. and Dominguez, R. (2014). Mechanism of IRSp53 inhibition and combinatorial activation by Cdc42 and downstream effectors. *Nat. Struct. Mol. Biol.* **21**, 413–422.

Kelly, G. M., Greenstein, P., Erezyilmaz, D. F. and Moon, R. T. (1995). Zebrafish wnt8 and wnt8b share a common activity but are involved in distinct developmental pathways. *Development* **121**, 1787–1799.

Kikuchi, A., Yamamoto, H., Sato, A. and Matsumoto, S. (2011). New insights into the mechanism of Wnt signaling pathway activation. *Int Rev Cell Mol Biol* **291**, 21–71.

Korkut, C., Ataman, B., Ramachandran, P., Ashley, J., Barria, R., Gherbesi, N. and Budnik, V. (2009). Trans-synaptic transmission of vesicular Wnt signals through Evi/Wntless. *Cell* **139**, 393–404.

Kornberg, T. B. and Roy, S. (2014). Cytonemes as specialized signaling filopodia. *Development* **141**, 729–736.

Kuhnert, F., Davis, C. R., Wang, H.-T., Chu, P., Lee, M., Yuan, J., Nusse, R. and Kuo, C. J. (2004). Essential requirement for Wnt signaling in proliferation of adult small intestine and colon revealed by adenoviral expression of Dickkopf-1. *Proceedings of the National Academy of Sciences* **101**, 266–271.

Laird D.J., Altshuler-Keylin S., Kissner M.D., Zhou X., Anderson K.V. (2011). Ror2 enhances polarity and directional migration of primordial germ cells. *PLoS Genet.* **7**, 12, :e1002428.

Liu, Y., Ross, J. F., Bodine, P. V. N. and Billiard, J. (2007). Homodimerization of Ror2 tyrosine kinase receptor induces 14-3-3(beta) phosphorylation and promotes osteoblast differentiation and bone formation. *Mol. Endocrinol.* **21**, 3050–3061.

Logan, C. Y. and Nusse, R. (2004). The Wnt signaling pathway in development and disease. *Annu. Rev. Cell Dev. Biol.* **20**, 781–810.

Luz, M., Spannl-Müller, S., Özhan, G., Kagermeier-Schenk, B., Rhinn, M., Weidinger, G. and Brand, M. (2014). Dynamic Association with Donor Cell Filopodia and Lipid-Modification Are Essential Features of Wnt8a during Patterning of the Zebrafish Neuroectoderm. *PLoS ONE* **9**, e84922.

Madan, B. and Virshup, D. M. (2015). Targeting Wnts at the source--new mechanisms, new biomarkers, new drugs. *Mol. Cancer Ther.* **14**, 1087–1094.

Mao, J., Fan, S., Ma, W., Fan, P., Wang, B., Zhang, J., Wang, H., Tang, B., Zhang, Q., Yu, X., et al. (2014). Roles of Wnt/β-catenin signaling in the gastric cancer stem cells proliferation and salinomycin treatment. *Cell Death Dis* **5**, e1039.

Mattes, B., Weber, S., Peres, J., Chen, Q., Davidson, G., Houart, C. and Scholpp, S. (2012). Wnt3 and Wnt3a are required for induction of the mid-diencephalic organizer in the caudal forebrain. *Neural Development* **7**, 12.

McGough, I. J. and Vincent, J.-P. (2016). Exosomes in developmental signalling. *Development* **143**, 2482–2493.

Mii, Y., Taira, M., Mii, Y. and Taira, M. (2009). Secreted Frizzled-related proteins enhance the diffusion of Wnt ligands and expand their signalling range. *Development* **136**, 4083–4088.

Mikels, A. J., Nusse, R., Nusse, R. and Mikels, A. J. (2006). Purified Wnt5a Protein Activates or Inhibits β-Catenin–TCF Signaling Depending on Receptor Context. *PLoS Biol* **4**, e115.

Mikels, A., Minami, Y. and Nusse, R. (2009). Ror2 receptor requires tyrosine kinase activity to mediate Wnt5A signaling. *Journal of Biological Chemistry* **284**, 30167–30176.

Moro, E., Ozhan-Kizil, G., Mongera, A., Beis, D., Wierzbicki, C., Young, R. M., Bournele, D., Domenichini, A., Valdivia, L. E., Lum, L., et al. (2012). In vivo Wnt signaling tracing through a transgenic biosensor fish reveals novel activity domains. *Dev. Biol.* **366**, 327–340.

Motoyama, T., Hojo, H. and Watanabe, H. (1986). Comparison of seven cell lines derived from human gastric carcinomas. *Pathology International* **36**, 65–83.

Mulligan, K. A., Fuerer, C., Ching, W., Fish, M., Willert, K. and Nusse, R. (2012). Secreted Wingless-interacting molecule (Swim) promotes long-range signaling by maintaining Wingless solubility. *Proc. Natl. Acad. Sci. U.S.A.* **109**, 370–377.

Nalbant, P., Hodgson, L., Kraynov, V., Toutchkine, A. and Hahn, K. M. (2004). Activation of endogenous Cdc42 visualized in living cells. *Science* **305**, 1615–1619.

Niehrs, C. (2012). The complex world of WNT receptor signalling. *Nat Rev Mol Cell Biol* **13**, 767–779.

Nishita, M., Yoo, S. K., Nomachi, A., Kani, S., Sougawa, N., Ohta, Y., Takada, S., Kikuchi, A. and Minami, Y. (2006). Filopodia formation mediated by receptor tyrosine kinase Ror2 is required for Wnt5a-induced cell migration. *The Journal of Cell Biology* **175**, 555–562.

Nusse, R. and Clevers, H. (2017). Wnt/β-Catenin Signaling, Disease, and Emerging Therapeutic Modalities. *Cell* **169**, 985–999.

Ohkawara, B. and Niehrs, C. (2011). An ATF2-based luciferase reporter to monitor non-canonical Wnt signaling in Xenopus embryos. *Dev. Dyn.* **240**, 188–194.

Oishi, I., Suzuki, H., Onishi, N., Takada, R., Kani, S., Ohkawara, B., Koshida, I., Suzuki, K., Yamada, G., Schwabe, G. C., et al. (2003). The receptor tyrosine kinase Ror2 is involved in non-canonical Wnt5a/JNK signalling pathway. *Genes Cells* **8**, 645–654.

Paganoni S., and Ferreira A. (2003). Expression and subcellular localization of Ror tyrosine kinase receptors are developmentally regulated in cultured hippocampal neurons. *J Neurosci Res*. **73**: 429-40.

Panáková, D., Sprong, H., Marois, E., Thiele, C. and Eaton, S. (2005). Lipoprotein particles are required for Hedgehog and Wingless signalling. *Nature* **435**, 58–65.

Pinto, D., Gregorieff, A., Begthel, H. and Clevers, H. (2003). Canonical Wnt signals are essential for homeostasis of the intestinal epithelium. *Genes Dev* **17**, 1709–1713.

Port, F. and Basler, K. (2010). Wnt trafficking: new insights into Wnt maturation, secretion and spreading. *Traffic* **11**, 1265–1271.

Rasmussen, N. R., Wright, T. M., Brooks, S. A., Hacker, K. E., Debebe, Z., Sendor, A. B., Walker, M. P., Major, M. B., Green, J., Wahl, G. M., et al. (2013). Receptor tyrosine kinase-like orphan receptor 2 (Ror2) expression creates a poised state of Wnt signaling in renal cancer. *Journal of Biological Chemistry* **288**, 26301–26310.

Rhinn, M., Lun, K., Luz, M., Werner, M. and Brand, M. (2005). Positioning of the midbrain-hindbrain boundary organizer through global posteriorization of the neuroectoderm mediated by Wnt8 signaling. *Development* **132**, 1261–1272.

Roarty, K., Pfefferle, A. D., Creighton, C. J., Perou, C. M. and Rosen, J. M. (2017). Ror2-mediated alternative Wnt signaling regulates cell fate and adhesion during mammary tumor progression. *Oncogene* **36**, 5958–5968.

Sagar, Pröls, F., Wiegreffe, C. and Scaal, M. (2015). Communication between distant epithelial cells by filopodia-like protrusions during embryonic development. *Development* **142**, 665–671.

Sailaja, B. S., He, X. C. and Li, L. (2016). The regulatory niche of intestinal stem cells. *J. Physiol. (Lond.)* **594**, 4827–4836.

Sato, A., Yamamoto, H., Sakane, H., Koyama, H. and Kikuchi, A. (2010). Wnt5a regulates distinct signalling pathways by binding to Frizzled2. *The EMBO Journal* **29**, 41–54.

Sato, M. and Kornberg, T. B. (2002). FGF is an essential mitogen and chemoattractant for the air sacs of the drosophila tracheal system. *Dev Cell* **3**, 195–207.

Schambony, A. and Wedlich, D. (2007). Wnt-5A/Ror2 regulate expression of XPAPC through an alternative noncanonical signaling pathway. *Dev Cell* **12**, 779–792.

Scholpp, S. and Brand, M. (2003). Integrity of the midbrain region is required to maintain the diencephalic-mesencephalic boundary in zebrafish no isthmus/pax2.1 mutants. *Dev. Dyn.* **228**, 313–322.

Scholpp, S., Delogu, A., Gilthorpe, J., Peukert, D., Schindler, S. and Lumsden, A. (2009). Her6 regulates the neurogenetic gradient and neuronal identity in the thalamus. *Proc. Natl. Acad. Sci. U.S.A.* **106**, 19895–19900.

Serralbo, O. and Marcelle, C. (2014). Migrating cells mediate long-range WNT signaling. *Development* **141**, 2057–2063.

Smutny, M., Ákos, Z., Grigolon, S., Shamipour, S., Ruprecht, V., Čapek, D., Behrndt, M., Papusheva, E., Tada, M., Hof, B., et al. (2017). Friction forces position the neural anlage. *Nature Publishing Group* **19**, 306–317.

Soille, P., Pesaresi, M. and Ouzounis, G. (2011). *Mathematical Morphology and Its Applications to Image and Signal Processing*. (eds. Soille, P., Pesaresi, M., and Ouzounis, G. K. Berlin, Heidelberg: Springer Science & Business Media.

Souren, M., Martinez-Morales, J. R., Makri, P., Wittbrodt, B. and Wittbrodt, J. (2009). A global survey identifies novel upstream components of the Ath5 neurogenic network. *Genome Biol.* **10**, R92.

Stanganello, E. and Scholpp, S. (2016). Role of cytonemes in Wnt transport. *J Cell Sci* **129**, 665–672.

Stanganello, E., Hagemann, A. I. H., Mattes, B., Sinner, C., Meyen, D., Weber, S., Schug, A., Raz, E. and Scholpp, S. (2015). Filopodia-based Wnt transport during vertebrate tissue patterning. *Nat Comms* **6**, 5846.

Surviladze, Z., Waller, A., Strouse, J. J., Bologa, C., Ursu, O., Salas, V., Parkinson, J. F., Phillips, G. K., Romero, E., Wandinger-Ness, A., et al. (2010). *A Potent and Selective Inhibitor of Cdc42 GTPase*. Bethesda (MD): National Center for Biotechnology Information (US).

Tada, M. and Heisenberg, C.-P. (2012). Convergent extension: using collective cell migration and cell intercalation to shape embryos. *Development* **139**, 3897–3904.

Takeuchi, S., Takeda, K., Oishi, I., Nomi, M., Ikeya, M., Itoh, K., Tamura, S., Ueda, T., Hatta, T., Otani, H., et al. (2000). Mouse Ror2 receptor tyrosine kinase is required for the heart development and limb formation. *Genes Cells* **5**, 71–78.

Takiguchi, G., Nishita, M., Kurita, K., Kakeji, Y. and Minami, Y. (2016). Wnt5a-Ror2 signaling in mesenchymal stem cells promotes proliferation of gastric cancer cells by activating CXCL16–CXCR6 axis. *Cancer Sci.* **107**, 290–297.

Valenta, T., Degirmenci, B., Moor, A. E., Herr, P., Zimmerli, D., Moor, M. B., Hausmann, G., Cantù, C., Aguet, M. and Basler, K. (2016). Wnt Ligands Secreted by Subepithelial Mesenchymal Cells Are Essential for the Survival of Intestinal Stem Cells and Gut Homeostasis. *Cell Rep* **15**, 911–918.

van Amerongen, R. and Nusse, R. (2009). Towards an integrated view of Wnt signaling in development. *Development* **136**, 3205–3214.

Voloshanenko, O., Gmach, P., Winter, J., Kranz, D. and Boutros, M. (2017). Mapping of Wnt-Frizzled interactions by multiplex CRISPR targeting of receptor gene families. *FASEB J.* **31**, 4832–4844.

Wallkamm, V., Dörlich, R., Rahm, K., Klessing, T., Nienhaus, G. U., Wedlich, D. and Gradl, D. (2014). Live Imaging of Xwnt5A-ROR2 Complexes. *PLoS ONE* **9**, e109428.

Winkel, A., Stricker, S., Tylzanowski, P., Seiffart, V., Mundlos, S., Gross, G. and Hoffmann, A. (2008). Wnt-ligand-dependent interaction of TAK1 (TGF-beta-activated kinase-1) with the receptor tyrosine kinase Ror2 modulates canonical Wnt-signalling. *Cellular Signalling* **20**, 2134–2144.

Witte, F., Bernatik, O., Kirchner, K., Masek, J., Mahl, A., Krejci, P., Mundlos, S., Schambony, A., Bryja, V. and Stricker, S. (2010). Negative regulation of Wnt signaling mediated by CK1-phosphorylated Dishevelled via Ror2. *FASEB J.* **24**, 2417–2426.

Yan, D. and Lin, X. (2008). Opposing roles for glypicans in Hedgehog signalling. *Nature Publishing Group* **10**, 761–763.

Yan, L., Du, Q., Yao, J. and Liu, R. (2016). ROR2 inhibits the proliferation of gastric carcinoma cells via activation of non-canonical Wnt signaling. *Exp Ther Med* **12**, 4128–4134.

Yang, Y. and Mlodzik, M. (2015). Wnt-Frizzled/planar cell polarity signaling: cellular orientation by facing the wind (Wnt). *Annu. Rev. Cell Dev. Biol.* **31**, 623–646.

Yeh, T. C., Ogawa, W., Danielsen, A. G. and Roth, R. A. (1996). Characterization and cloning of a 58/53-kDa substrate of the insulin receptor tyrosine kinase. *J Biol Chem* **271**, 2921–2928.

Yoda, A., Oishi, I. and Minami, Y. (2003). Expression and function of the Ror-family receptor tyrosine kinases during development: lessons from genetic analyses of nematodes, mice, and humans. *J. Recept. Signal Transduct. Res.* **23**, 1–15.

Yu, J., Chia, J., Canning, C. A., Jones, M., Bard, F. A. and Virshup, D. M. (2014). WLS retrograde transport to the endoplasmic reticulum during Wnt secretion. *Dev Cell* **29**, 277–291.

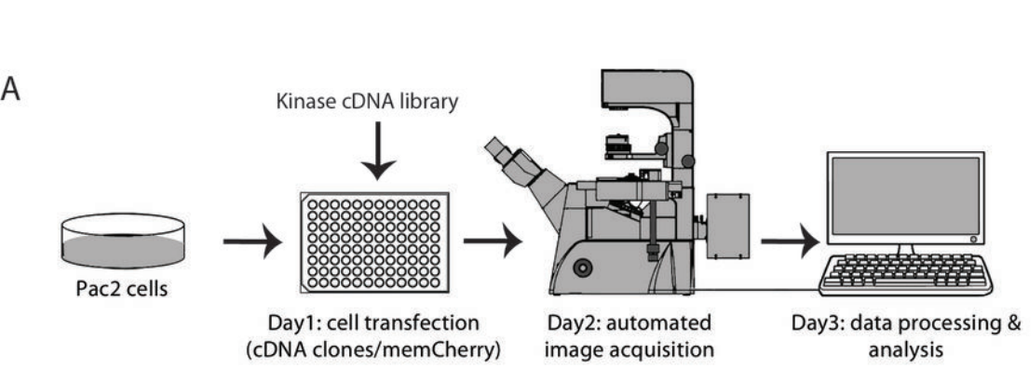

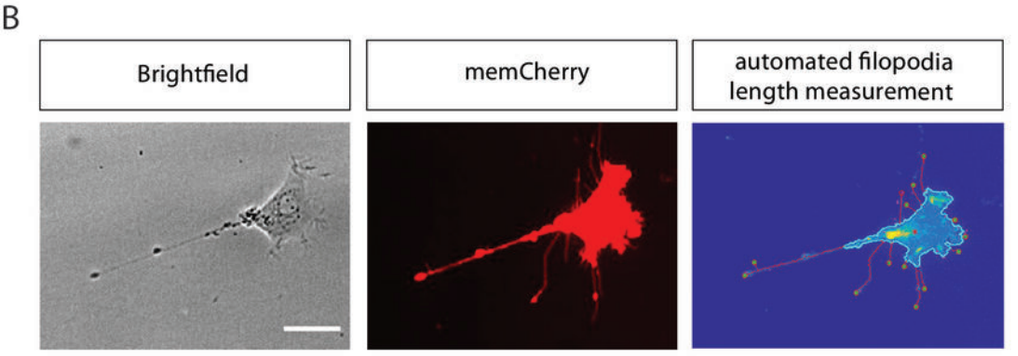

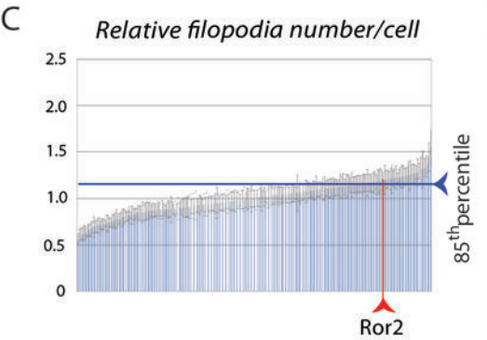

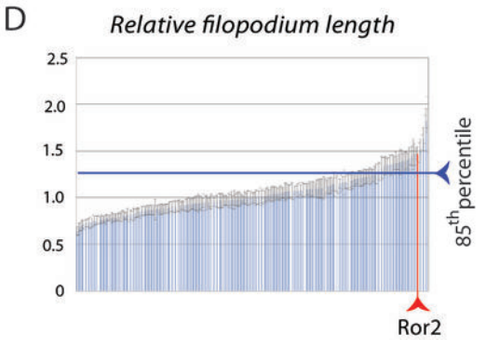

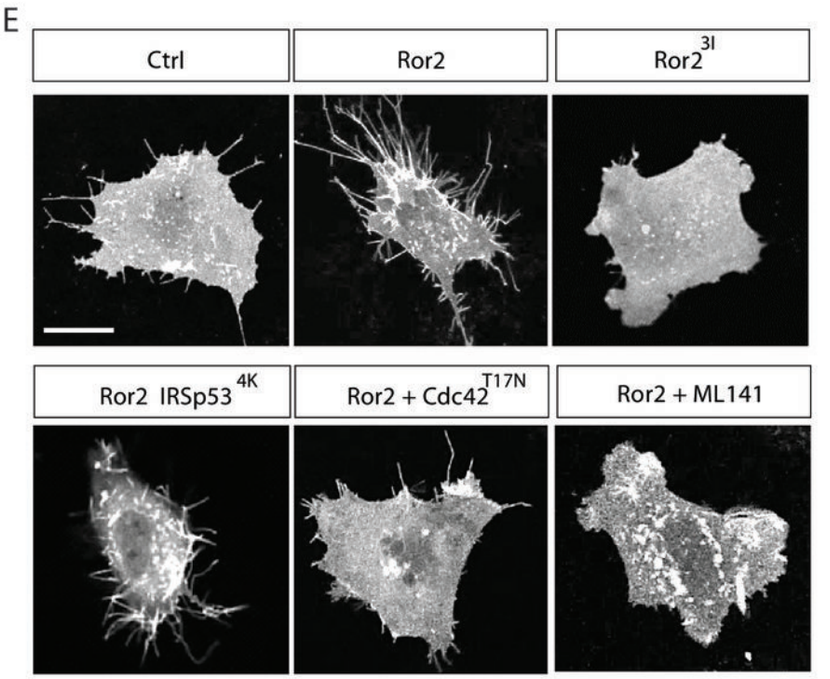

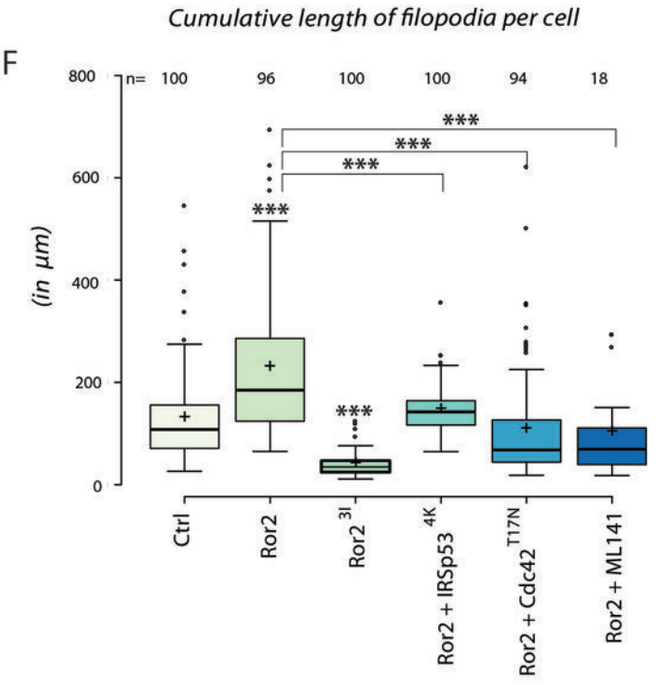

Figure 1; Mattes et al., 2018

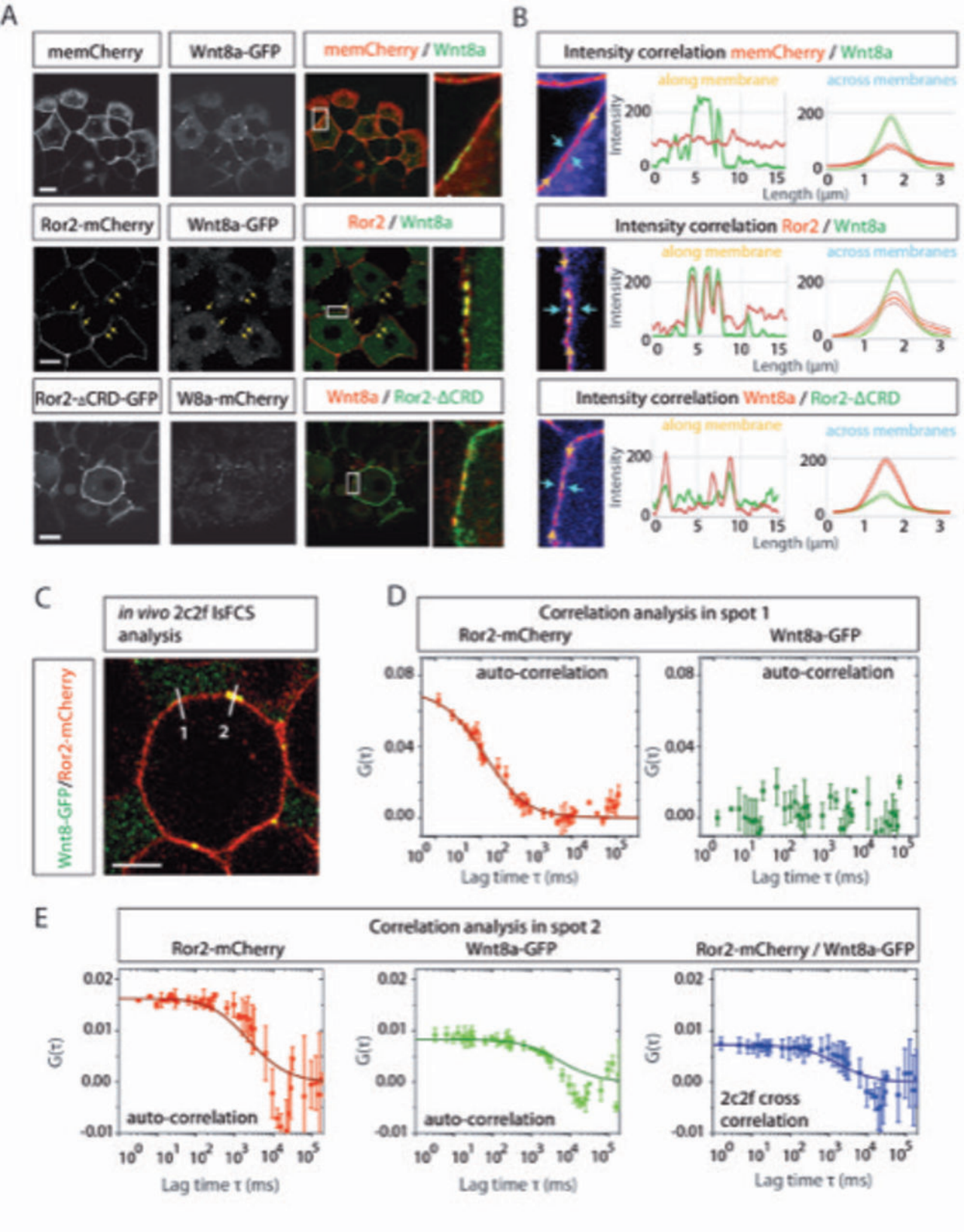

Figure 2; Mattes et al., 2018

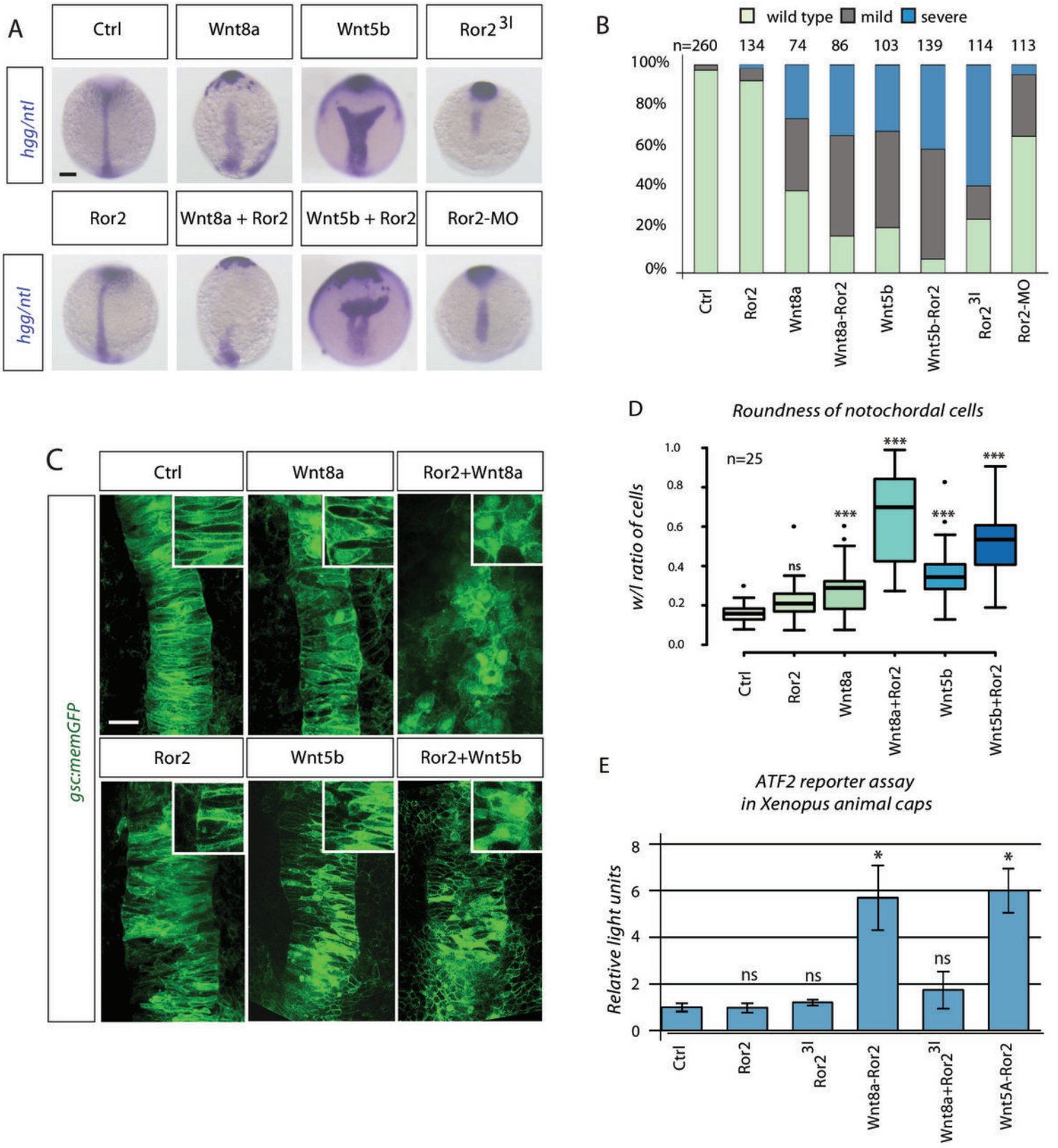

Figure 3; Mattes et al., 2018

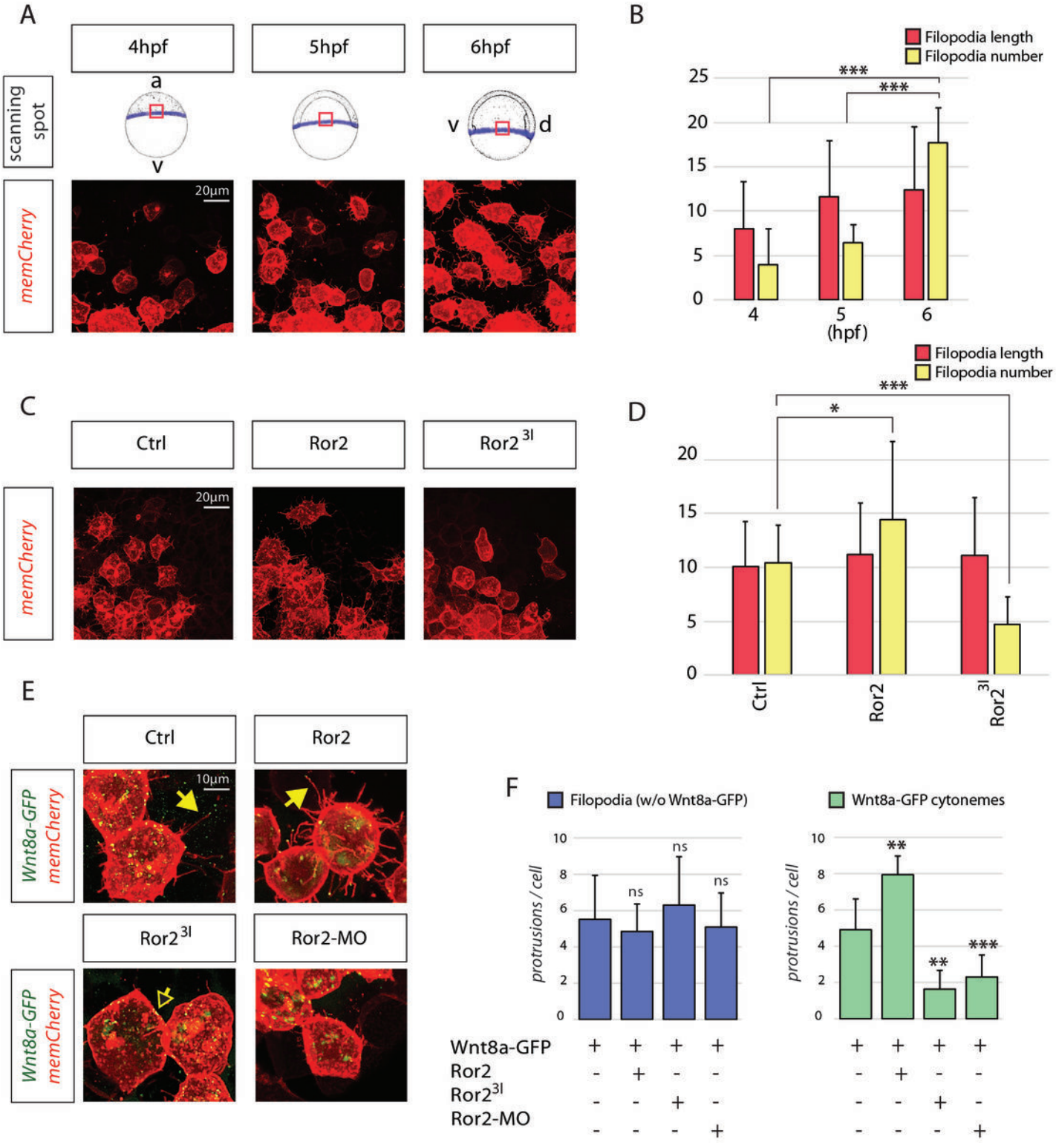

Figure 4; Mattes et al., 2018

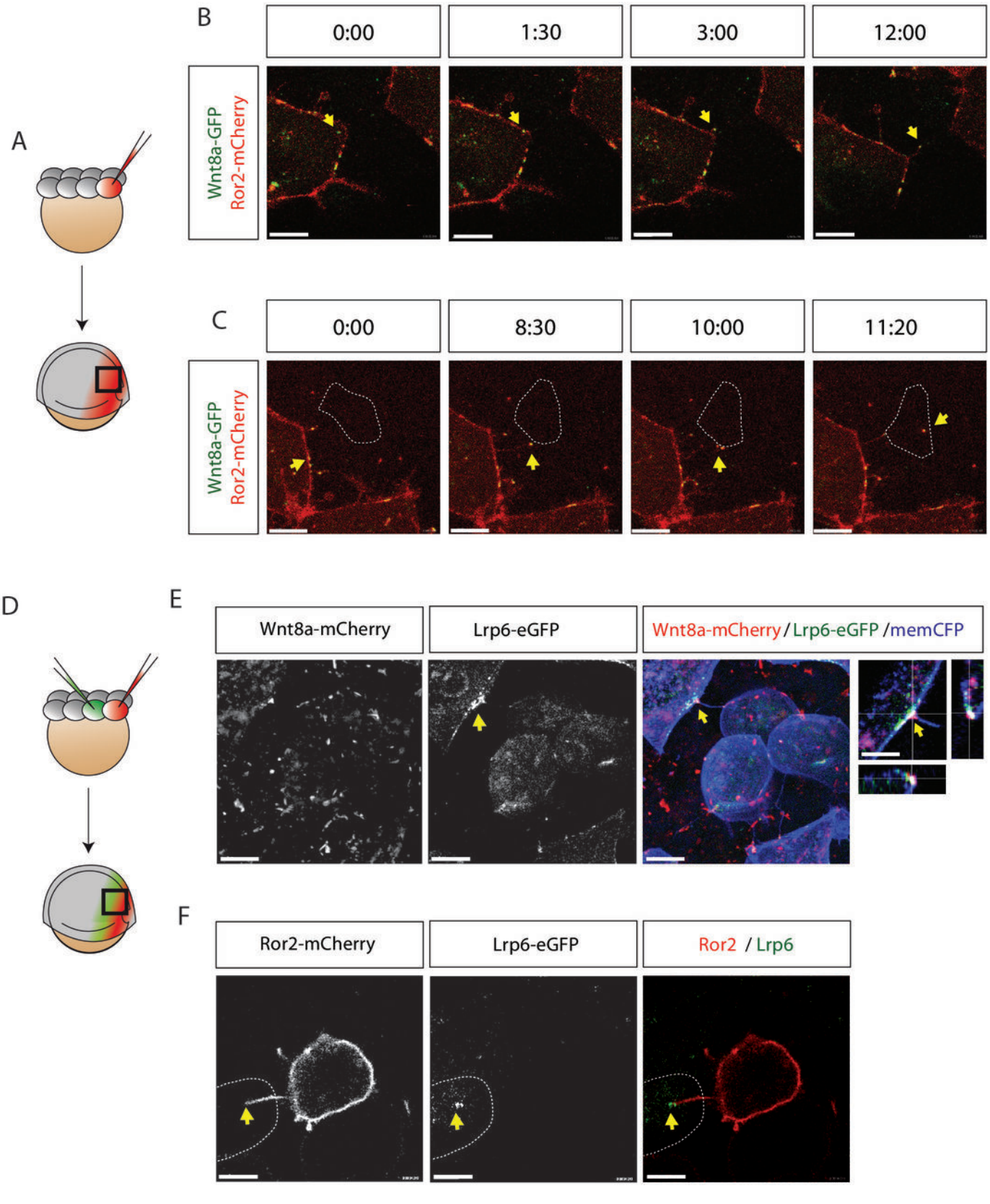

Figure 5; Mattes et al., 2018

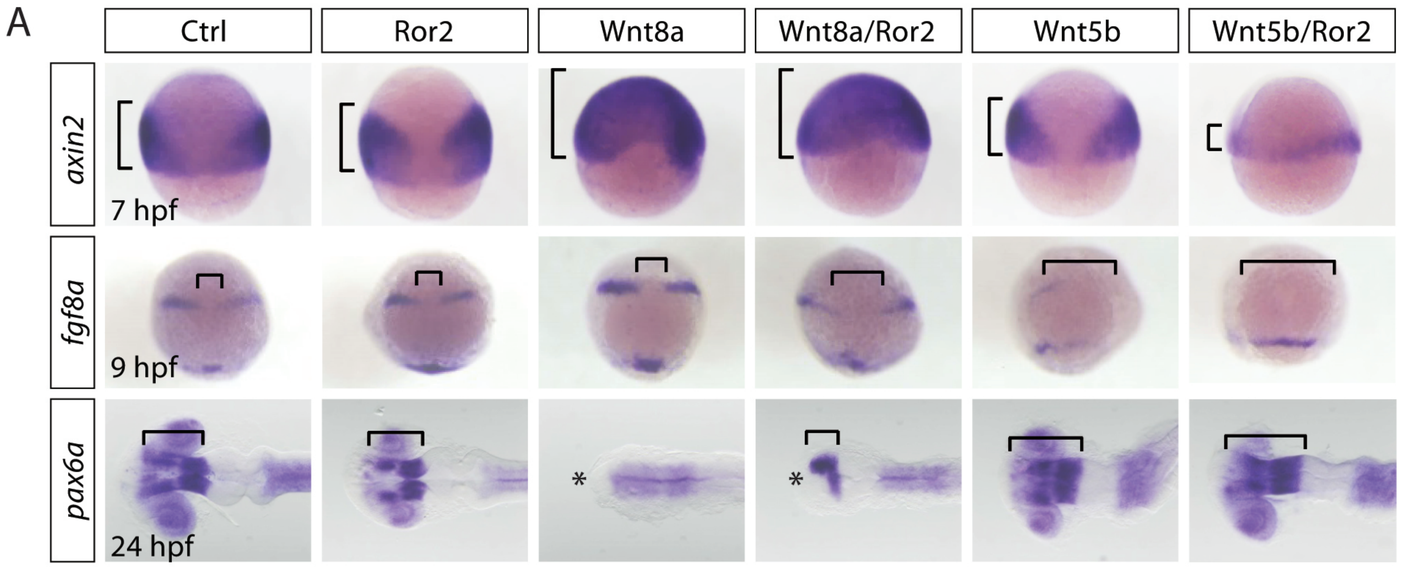

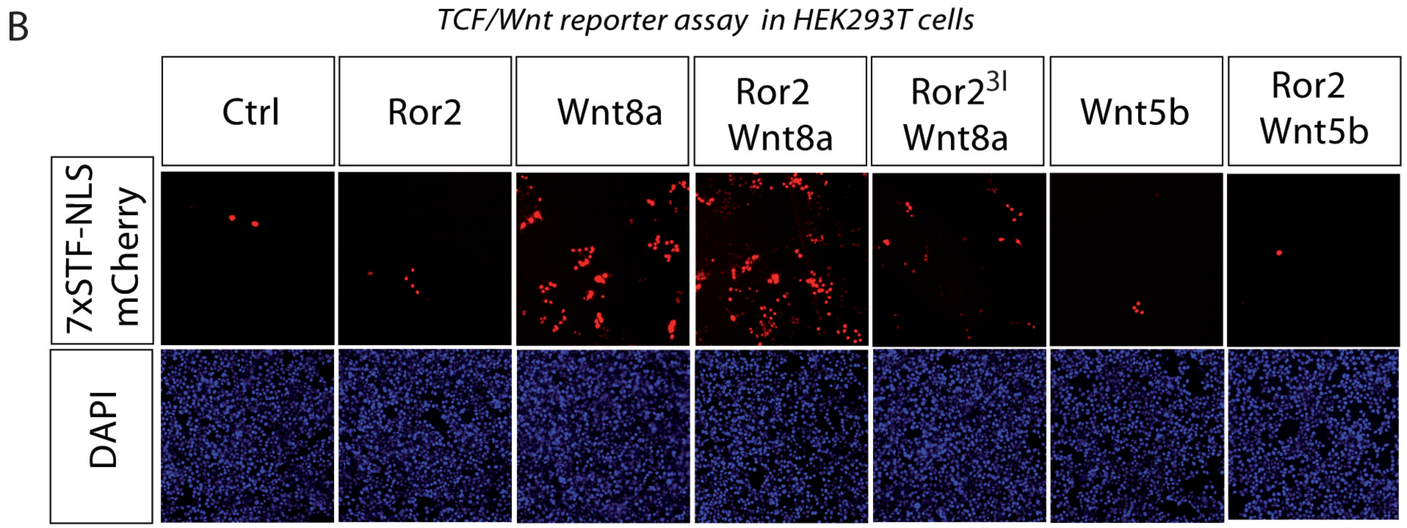

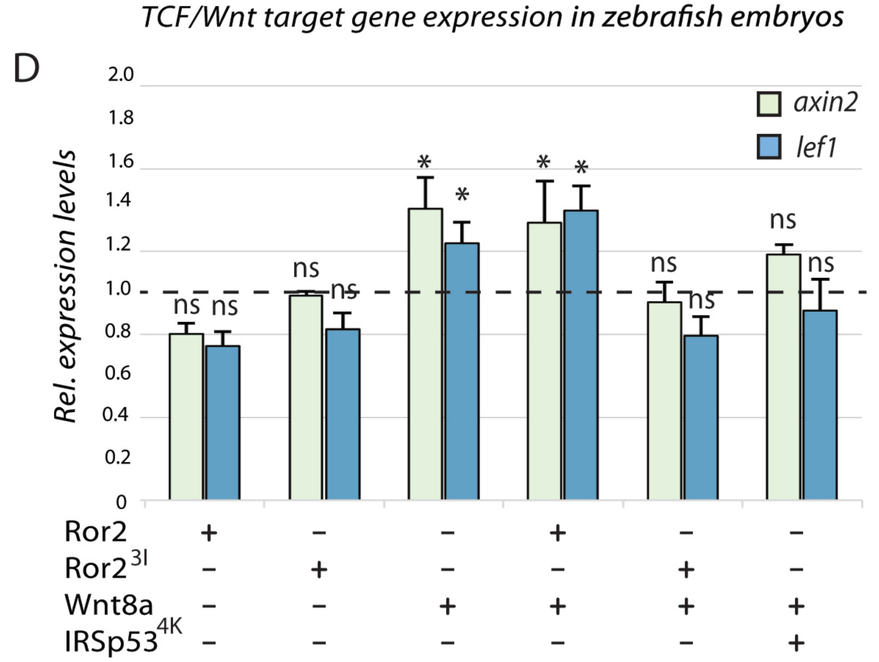

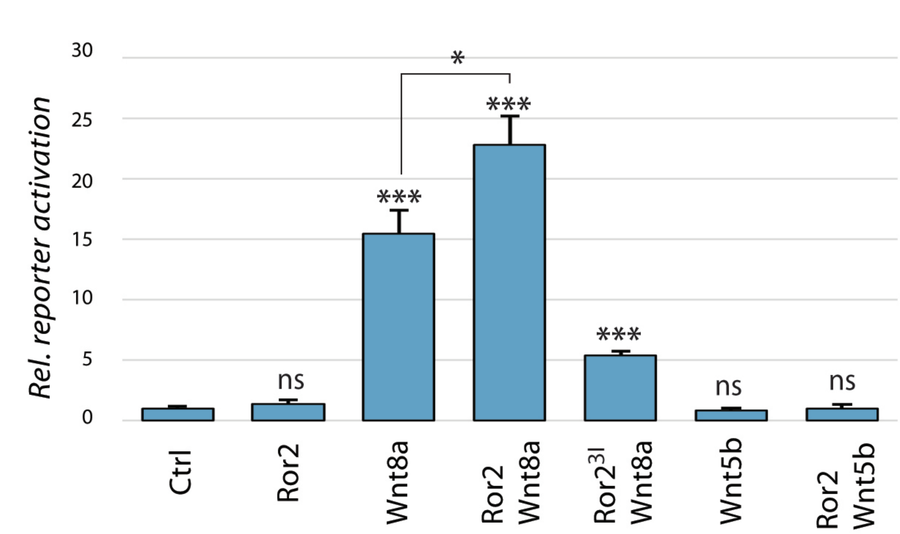

Figure 6; Mattes et al., 2018

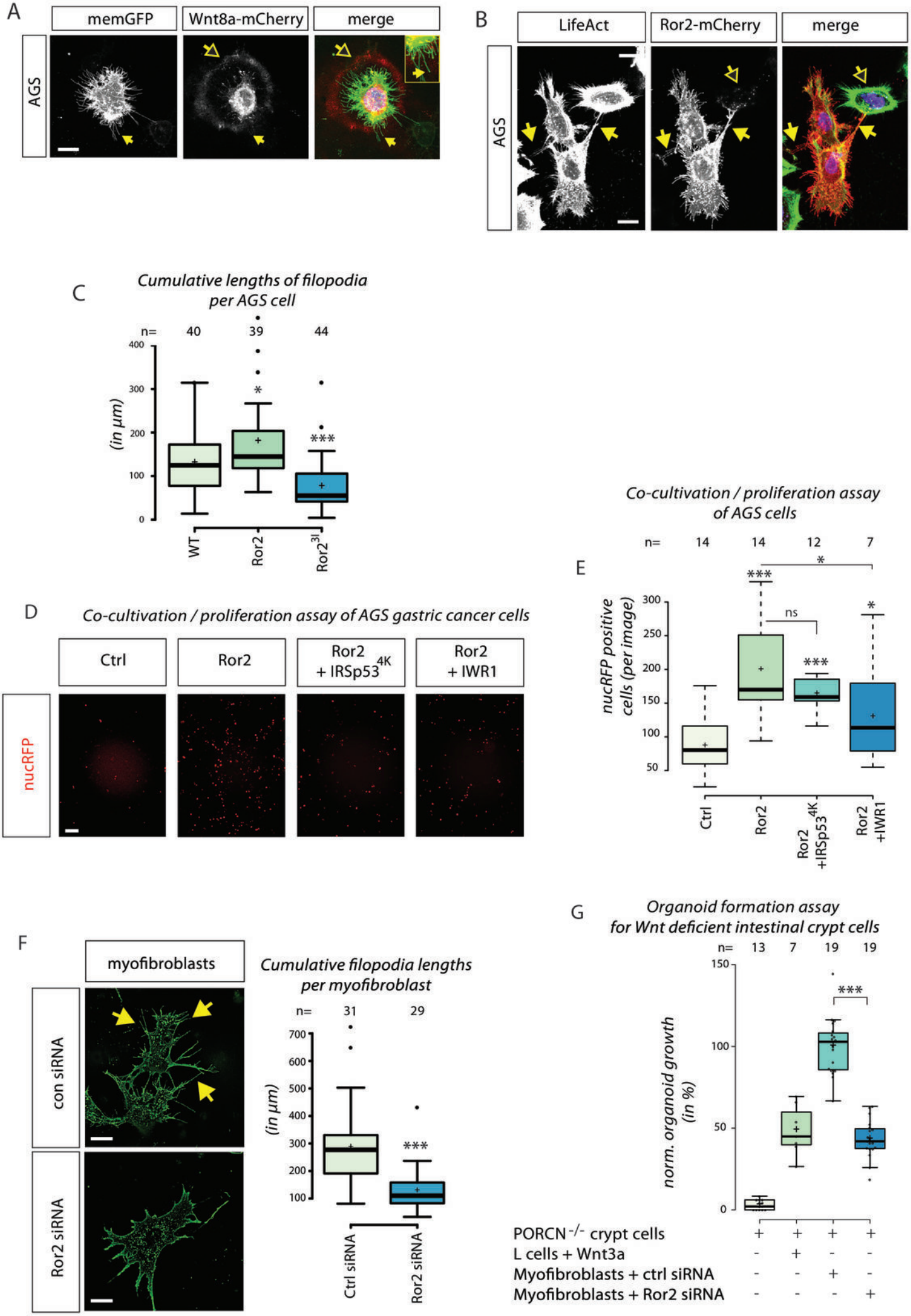

Figure 7; Mattes et al., 2018

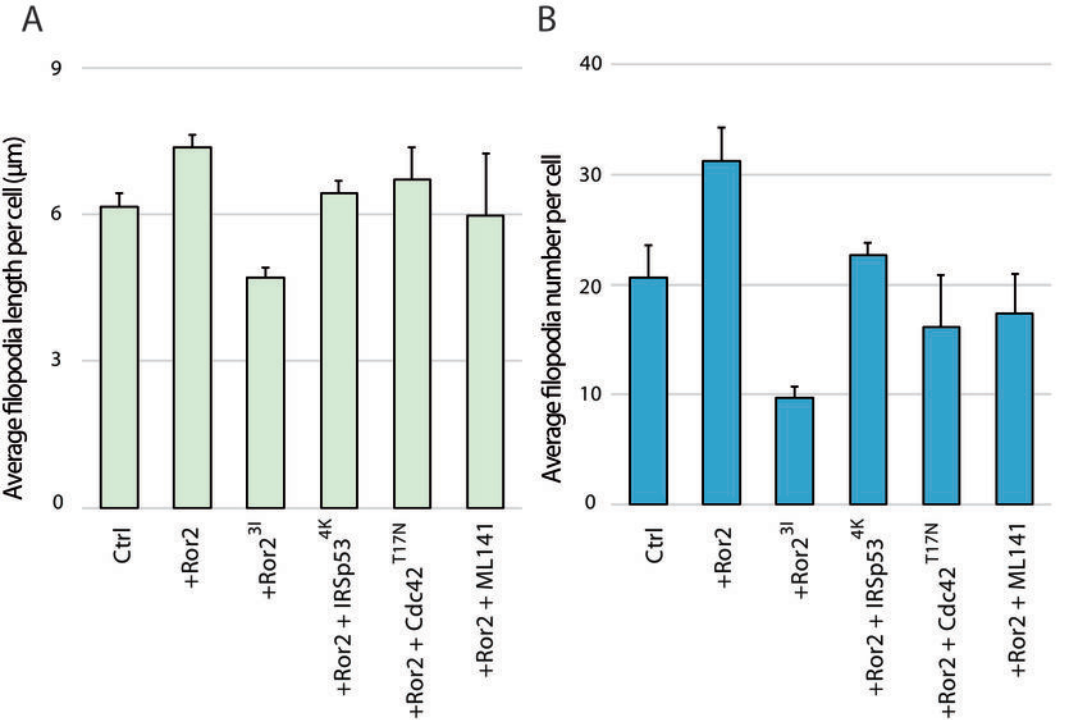

Supplementary Figure 1; Mattes et al., 2017

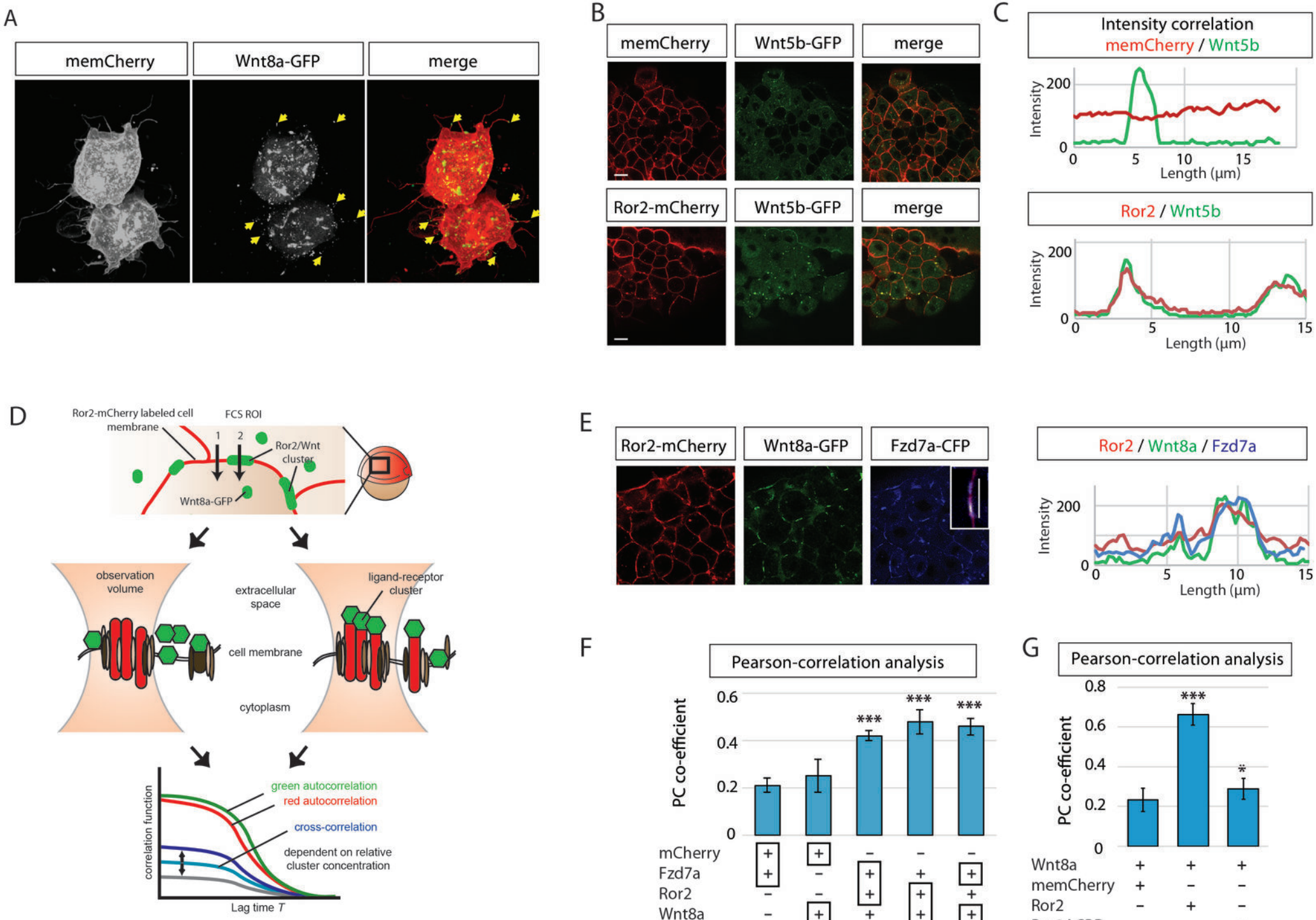

Supplementary Figure 2; Mattes et al., 2018

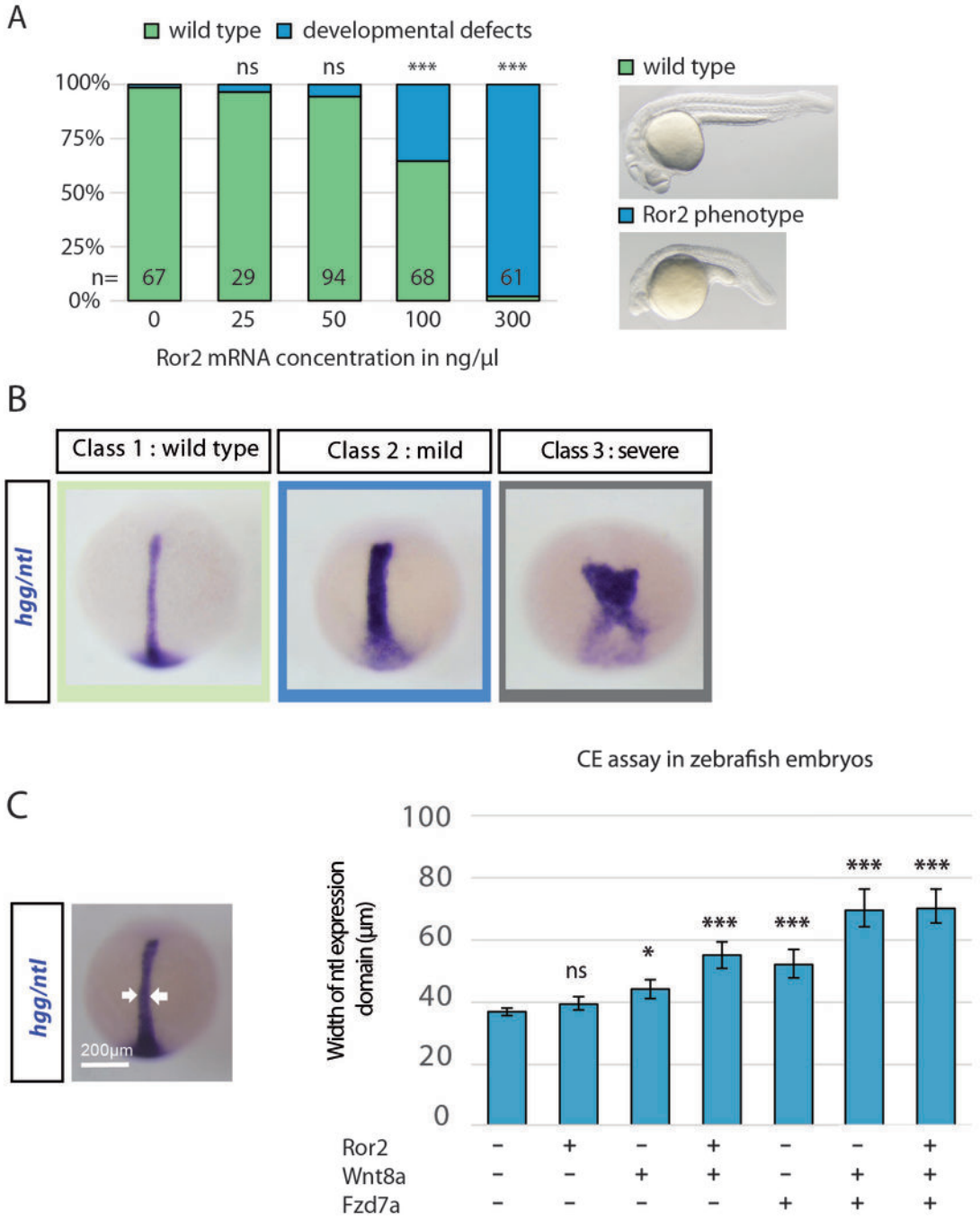

Supplementary Figure 3; Mattes et al., 2018

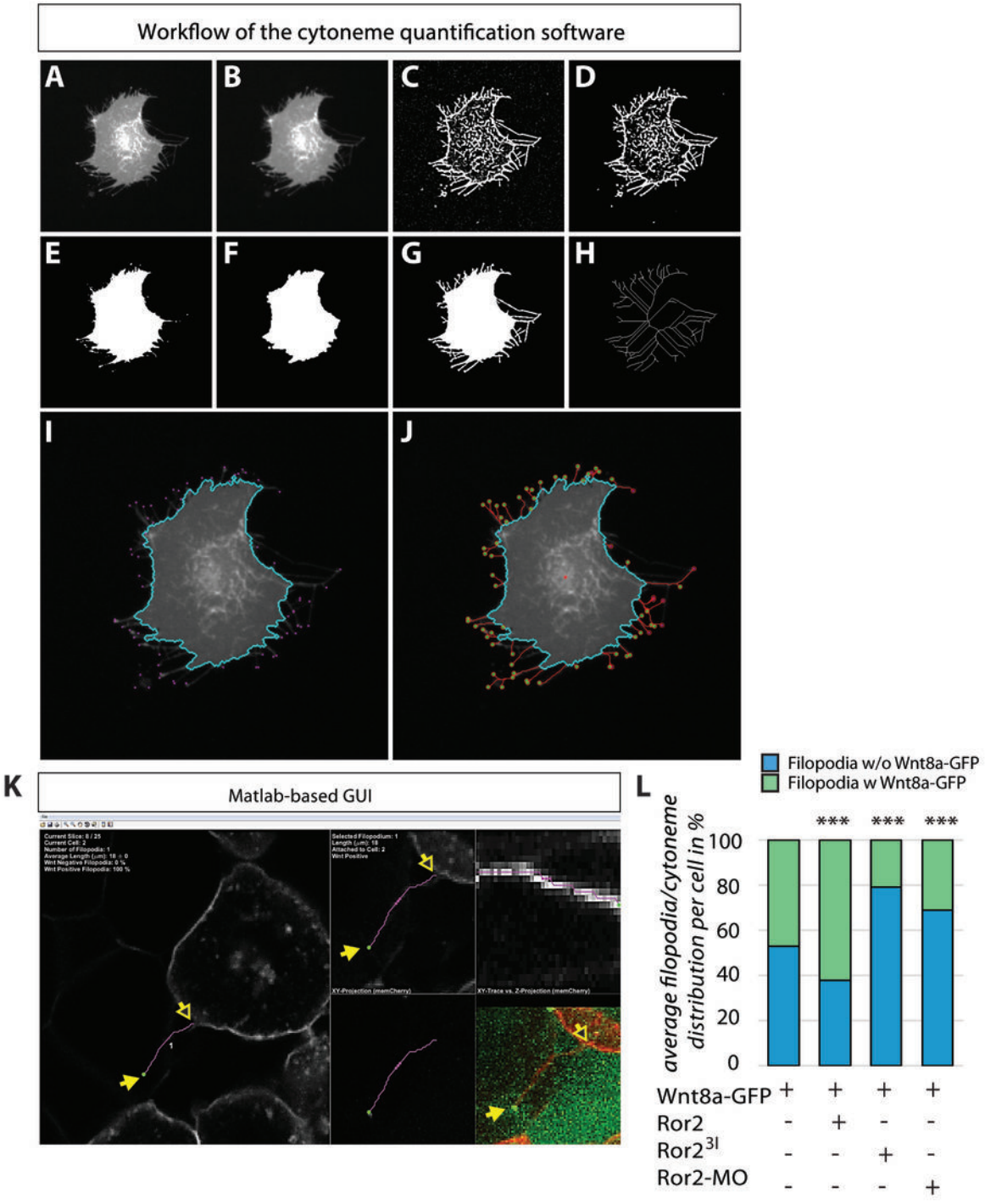

Supplementary Figure 3; Mattes et al., 2018

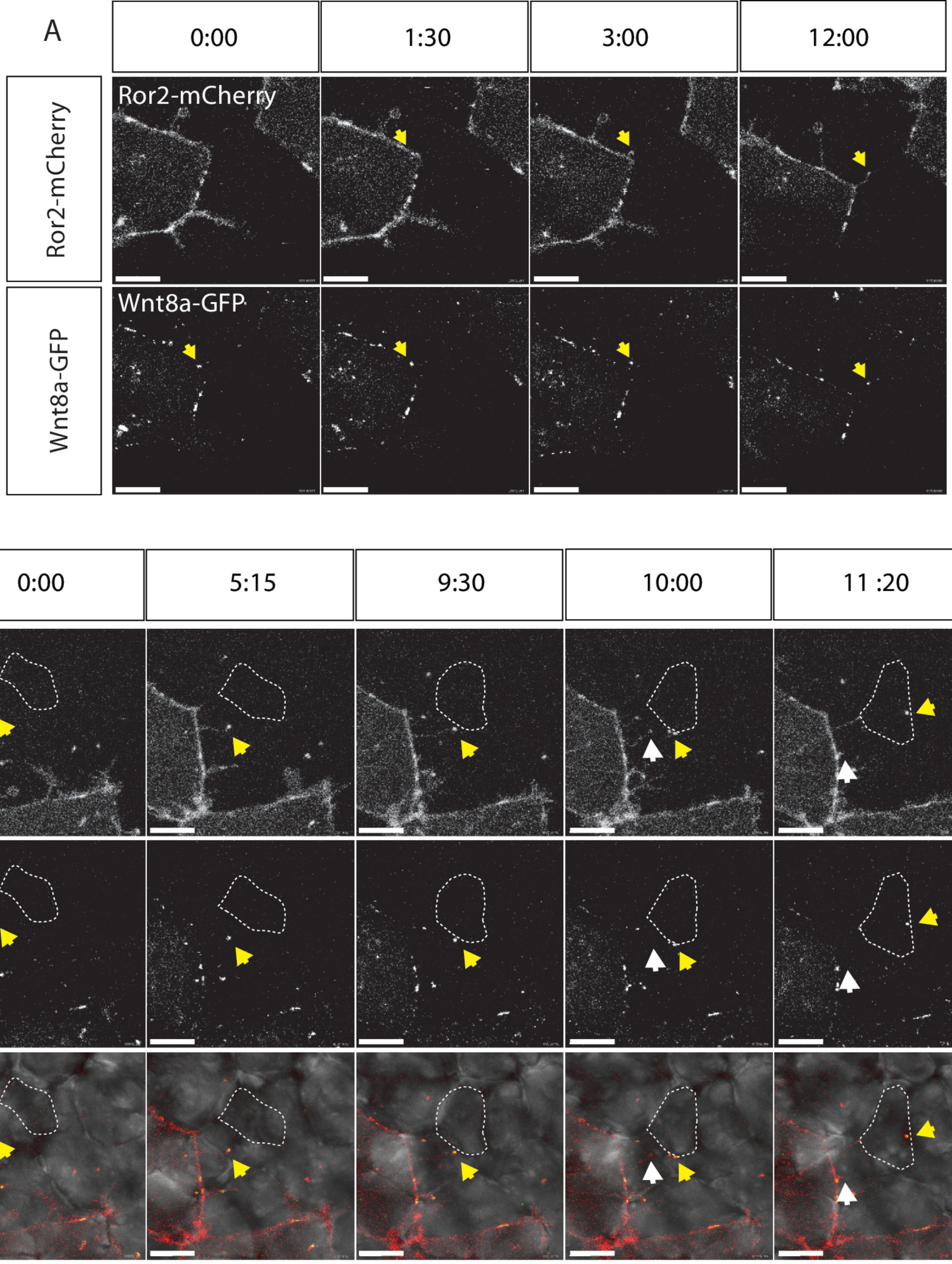

Supplementary Figure 5; Mattes et al., 2018

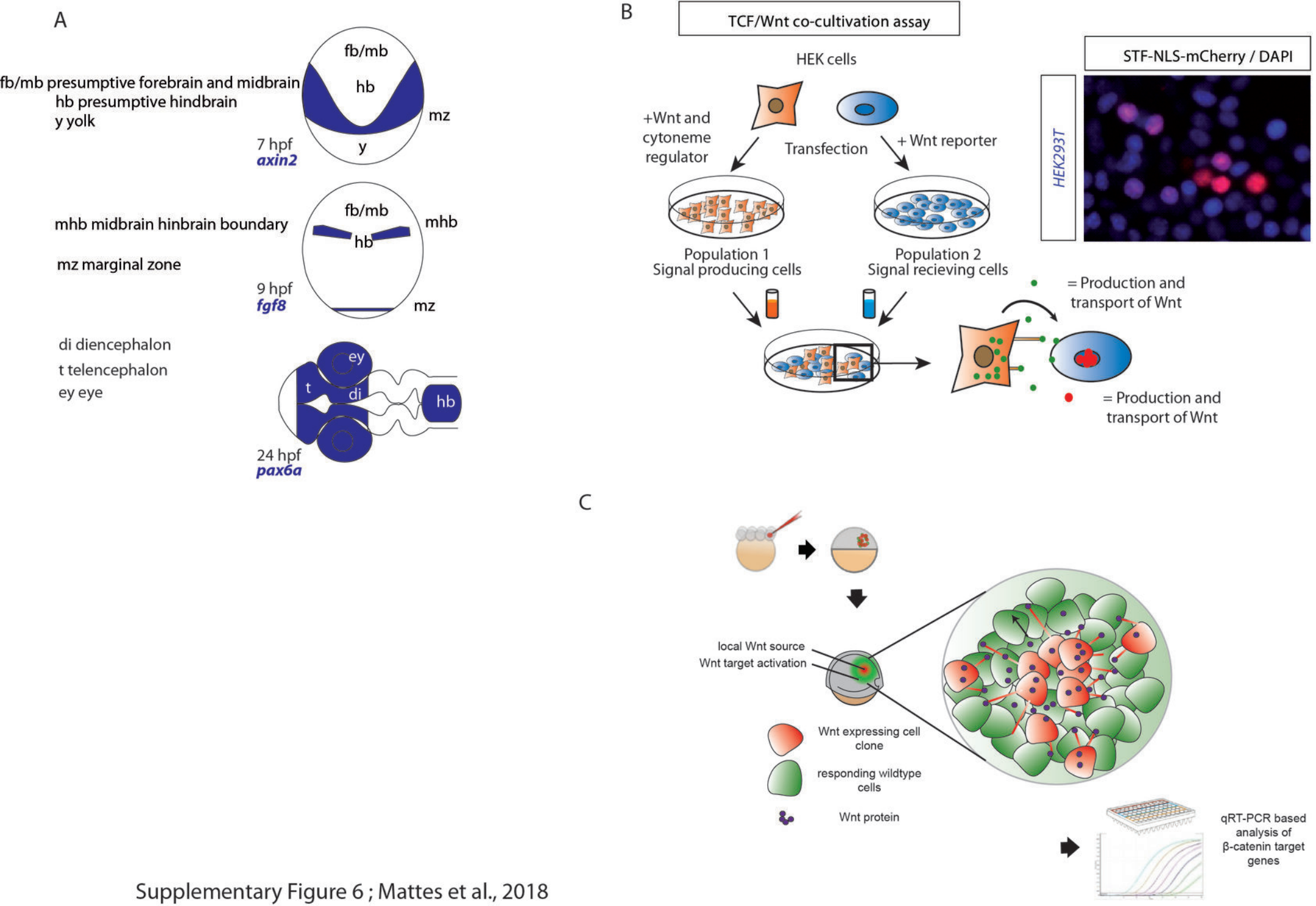

Supplementary Figure 6 ; Mattes et al., 2018

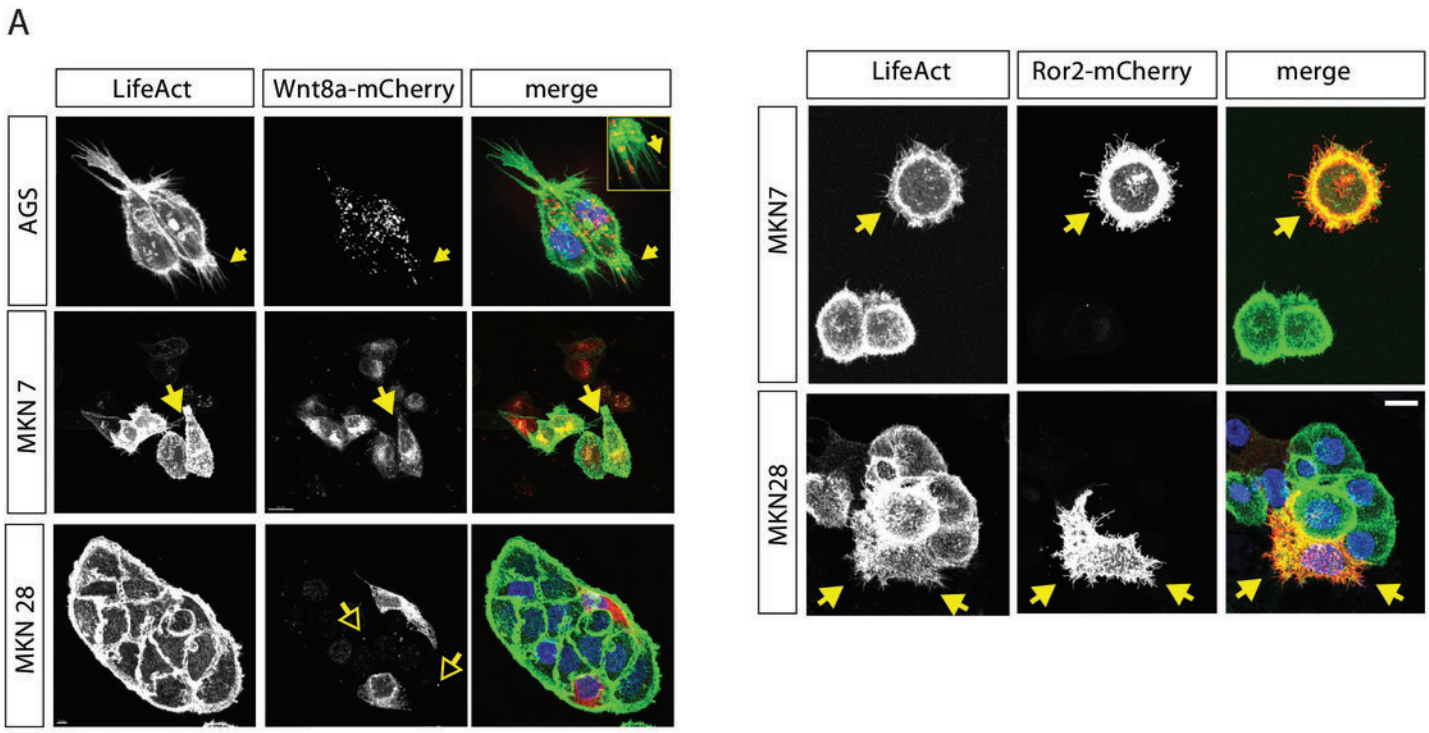

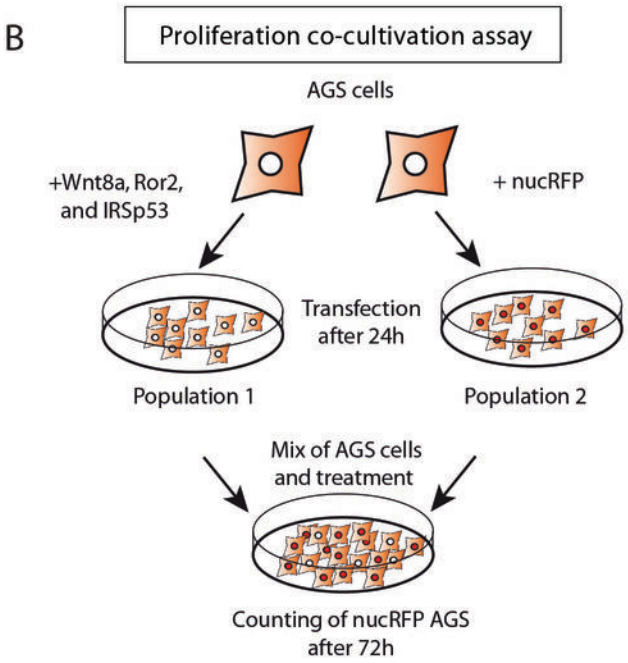

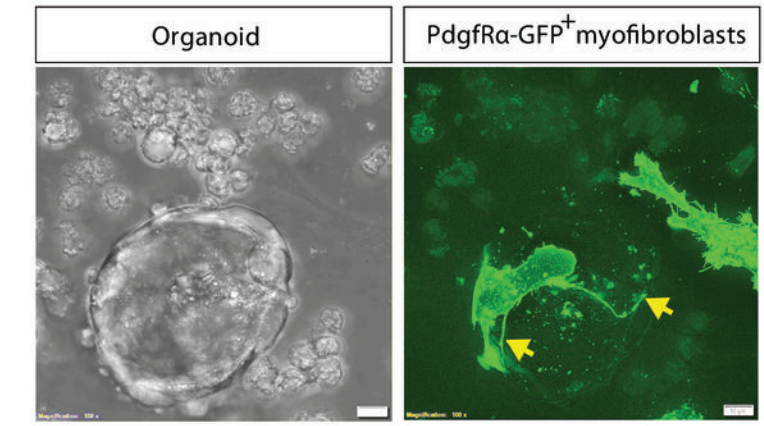

Supplementary Figure 7; Mattes et al., 2018